STATE OF POLAR CLIMATE

2024

CHINESE ACADEMY OF METEOROLOGICAL SCIENCES

STATE OF POLAR CLIMATE

(2024)

CHINESE ACADEMY OF METEOROLOGICAL SCIENCES

2025.03

Editorial Committee for State of Polar Climate 2024

Abstract

In 2024, the temperature of the Antarctic continent was slightly higher than normal, with significant differences between the eastern and western regions and distinct seasonal variations. From 1979 to 2024, the warming rate of the Antarctic land was 0.20°C per decade, slightly higher than the global average. The annual average temperature of the Antarctic continent in 2024 was -31.79°C, 0.05°C higher than normal. A persistent warm event occurred in Queen Maud Land, while Wilkes Land remained continuously cold. The winter temperature at Syowa Station reached a record high, and the annual temperature at Neumayer Station ranked third highest in history. The inland Dome and Victoria Land showed a pattern of "cold summers and warm winters". The average winter temperature at Vostok Station was 4.34°C higher than normal, setting a new historical record.

The Arctic region continued to warm, with the Canadian Arctic experiencing persistent extreme warmth. The warming rate in the Arctic was 2.9 times that of the global average (0.18°C per decade) during the same period. The annual average temperature in the Arctic region in 2024 was -6.89°C, 0.65°C higher than normal. The average temperatures in spring, summer, autumn, and winter were -10.33°C, 6.51°C, -4.99°C, and -19.37°C, respectively, with unusually warm autumn and winter. Alaska and the Canadian Arctic continued to be the major warming centers. The temperature at Deadhorse station reached 31.7°C on August 6, and the temperature at Inuvik reached 34.8°C on August 7. In August 2024, the overall sea surface temperature of the Arctic Ocean was higher than normal, but the regional temperature difference was significant: the Barents Sea reached a record high, while the Chukchi Sea reached a record low.

In 2024, the Antarctic sea ice remained at a low level, and the continuous reduction of Arctic sea ice. On February 20, 2024, the extent of Antarctic sea ice reached its annual minimum of 1.97×10^6 km², the third lowest on record after 2023 and 2022. The annual cumulative and maximum sea ice extents were slightly higher than the lowest record in 2023, ranking second lowest. In particular, the sea ice extent in November 2024 set a 46 year low for that month. The minimum extent of Arctic sea ice in 2024 ranked seventh lowest in history, at 4.21×10^6 km²; the annual cumulative sea ice extent ranked sixth lowest; and the sea ice extent in December 2024 set a 46 year low for that month.

The development of the Antarctic ozone hole in 2024 was relatively stable, while the total ozone amount in the Arctic showed abnormal increases. This represented a moderation compared to the phenomenon of an abnormally large and persistent Antarctic ozone hole area from 2019 to 2023. On September 28, the ozone hole reached its single-day maximum coverage area of approximately

2.2×10^7 km², smaller than the 2.5×10^7 km^2 in 2023, with both the maximum coverage area and the opening/closing timing being closer to the average levels from 1979 to 2021. In the Arctic region, the weakening of the polar vortex due to reduced upward propagation of large-scale planetary waves in winter led to abnormal ozone increases. The ozone column concentration hit a historical high of 477 Dobson Units (DU) in March 2024, which was 14.5% higher than the average from 1979 to 2023.

The concentrations of greenhouse gases in the polar atmosphere showed a similar trend to global changes, all showing a stable upward trend. In 2023, the annual average concentrations of carbon dioxide, methane, nitrous oxide, and sulfur hexafluoride in the Antarctic atmosphere were 416.39 ppm, 1870.60 ppb, 335.70 ppb, and 11.15 ppt, respectively. In 2023, the annual average concentrations of carbon dioxide, methane, nitrous oxide, and sulfur hexafluoride in the Arctic atmosphere were 422.06 ppm, 2013.75 ppb, 337.03 ppb, and 11.69 ppt, respectively. Compared with 2022, the average concentrations of major greenhouse gases in the polar atmosphere increased.

Contents

Chapter 1 Temperature and Air pressure

1.1 Air Temperature

1.1.1 Antarctic

This subsection analyzes temperature observations from multiple stations in Antarctica, along with first-generation global atmospheric reanalysis data (CMA-RA) released by the National Meteorological Information Center. Temperature observations from Great Wall and Zhongshan Stations are sourced from the Chinese Academy of Meteorological Sciences, while additional data are obtained from the Reference Antarctic Data for Environmental Research (Met-READER) compiled by the British Antarctic Survey. All datasets have undergone stringent quality control.

The analysis results indicate that the annual average temperature for the Antarctic continent in 2024 was -31.79°C, which is slightly above the long-term average by 0.05°C. In terms of seasonal distribution, the average temperatures for the austral summer (December to February), autumn (March to May), winter (June to August), and spring (September to November) were -22.65°C, -35.67°C, -36.64°C, and -33.00°C, respectively. Notably, in 2024, the Antarctic continent experienced cooler temperatures during the austral summer, autumn, and spring compared to the long-term average, with decreases of 1.04°C, 0.57°C, and 0.60°C, respectively. In contrast, winter exhibited a warm anomaly, with an increase of 1.60°C.

Similar to 2023, the Antarctic continent in 2024 experienced warmer conditions in the Coats Land and Queen Maud Land regions, while the Wilkes Land area was cooler (see Figure 1.1). Specifically, the annual temperature at the Nomaiyr Station in Queen Maud Land was 1.43°C above the long-term average, marking the third highest recorded temperature (Figure 1.1-27). Additionally, winter temperatures in Queen Maud Land were exceptionally high, with Showa Station recording a temperature increase of 3.28°C, setting a new historical record (Figure 1.1-25). In contrast, Wilkes Land was overall cooler in 2024, primarily due to lower autumn temperatures compared to the long-term average. At the Dimon-Divier Station, autumn temperatures were 2.19°C below average, reaching the second lowest on record (Figure 1.1-17).

For other regions, although the annual temperature anomalies were relatively weak, they displayed apparent seasonal variations. For instance, Victoria Land and the interior of Antarctica exhibited a “cool summer, warm winter” pattern. During summer, temperatures in these areas were below average, with Marilyn Station and East Station recording summer temperatures that were 2.84°C and 2.72°C lower than normal, respectively, both setting historical lows for summer temperatures (see Figures 1.1-12 and 20). In contrast, winter temperatures in these areas were higher than average, with Vostok Station’s winter temperature exceeding normal by 4.34°C, establishing a new record. Amundsen-Scott Station and Manuela Station also recorded winter temperatures that were above average by 4.39°C and 2.18°C, reaching the second highest in history (see Figures 1.1-20, 21, and 16). The annual average temperature on the Antarctic Peninsula remained roughly in line with long-term averages. However, spring temperatures in the northern part of the peninsula were notably lower, with O’Higgins Station recording a spring temperature that was

1.90°C below normal, marking the third lowest on record (see Figure 1.1-4).

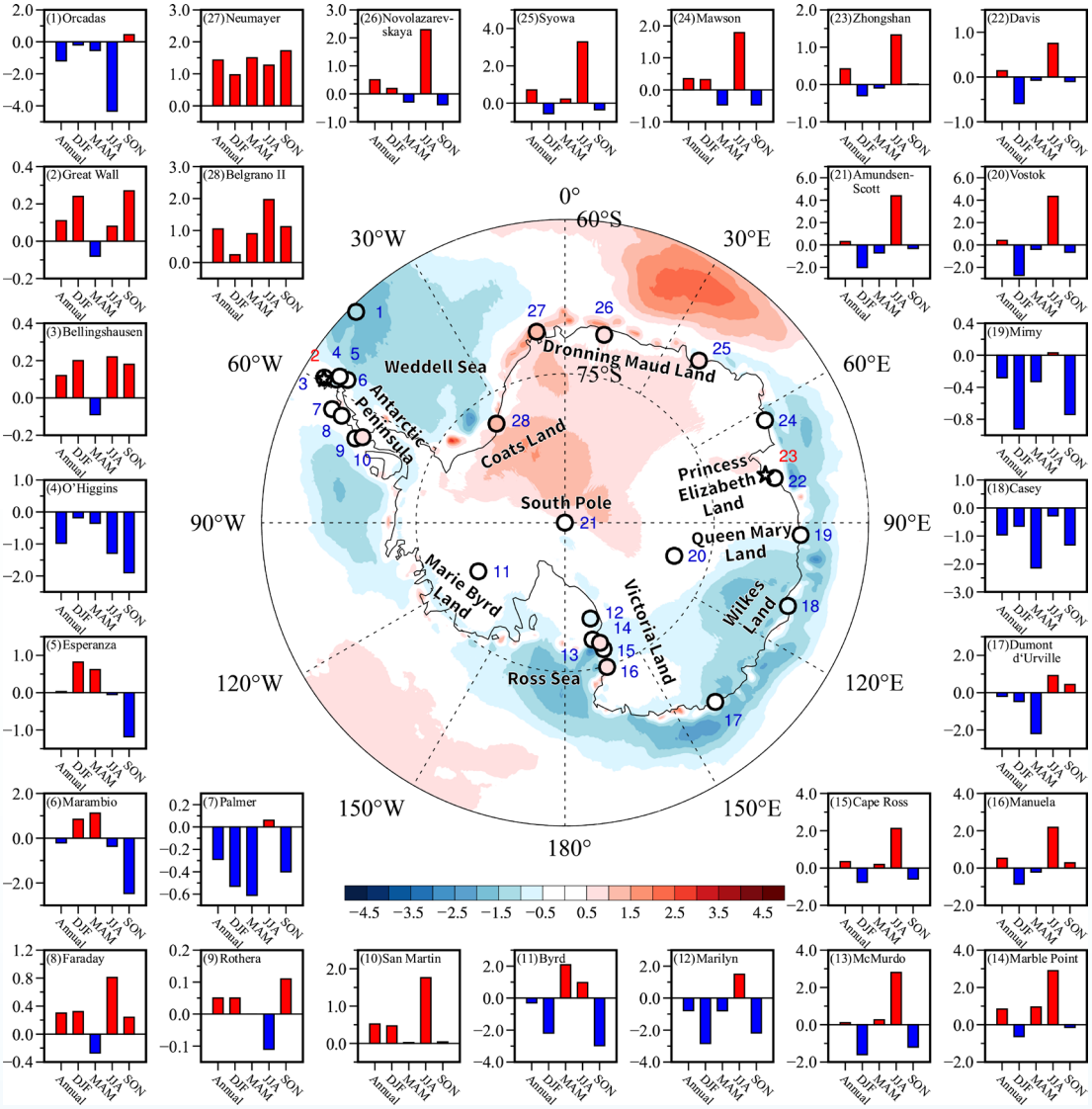

Figure 1.1 Spatial distribution of the 2024 annual mean temperature anomalies in Antarctica and the annual and seasonal mean temperature anomalies at various stations (unit: °C)

From 1979 to 2024, global air temperature exhibited a significant warming trend, with the rate of 0.18°C per decade (Figure 1.2). Under this global warming background, the warming trend in Antarctica was primarily over the Antarctic continent (ice sheet), where the warming rate slightly exceeded the global average, reaching 0.20°C per decade (Figure 1.2). Additionally, there were remarkable differences in seasonal air temperature trends. During the austral summer and autumn, air temperatures showed a significant warming trend, with rates of 0.26°C per decade and 0.31°C per decade, respectively ($p < 0.05$). However, in spring and winter, the warming trend was relatively weaker, at 0.14°C per decade and 0.11°C per decade respectively, and did not pass the significance test ($p > 0.1$).

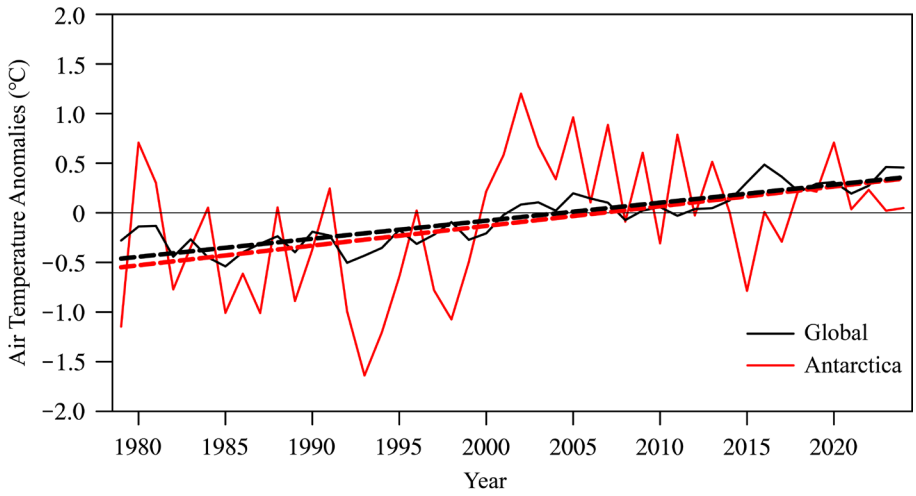

Figure 1.2 Time series of annual mean surface temperature anomalies averaged over Antarctic Continent (solid red line) and globally (solid black line) from 1979 to 2024, along with their trends (dashed lines) (unit: °C)

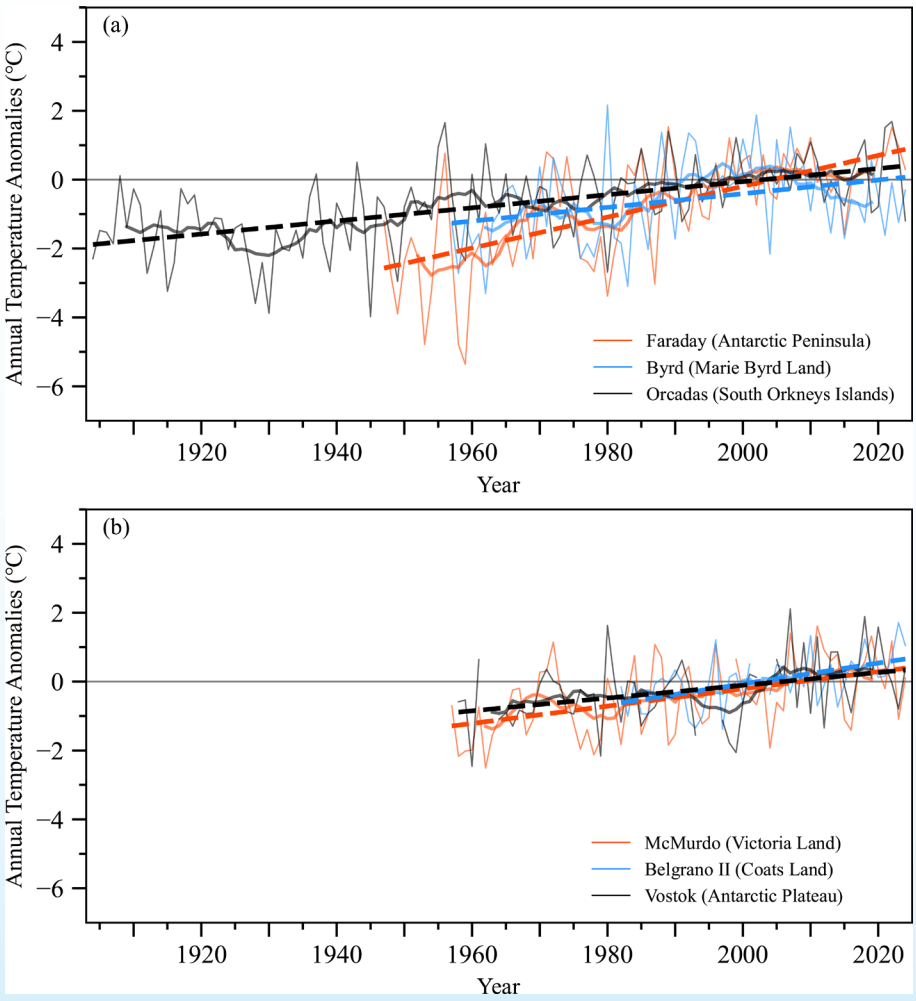

Figure 1.3 Time series of annual mean temperature anomalies at warming sites in the West Antarctic (a) and East Antarctic (b) regions. The thin solid line represents the annual mean temperature anomalies, the thick solid line represents the 11-year running average of annual mean temperature anomalies, and the dashed line indicates the trend in annual mean temperature anomalies

The temperature trend in Antarctic continent reveals distinct regional characteristics, with certain areas displaying high sensitivity to climate change. For instance, the West Antarctic region continues to experience significant warming, with the Antarctic Peninsula standing out as one of the most rapidly warming regions globally. Specifically, at the Faraday station, the annual temperature has been rising at a rate of 0.45°C per decade (1947-2024, depicted by the red line in Figure 1.3a). Additionally, the annual temperatures in the South Orkney Islands, Marie Byrd Land, Victoria Land, Coats Land, and the Antarctic Dome also exhibit a warming trend, albeit at a slower pace, with warming rates of 0.19°C per decade (1904-2023, black line in Figure 1.3a), 0.20°C per decade (1957-2024, blue line in Figure 1.3a), 0.25°C per decade (1957-2024, red line in Figure 1.3b), 0.30°C per decade (1982-2024, blue line in Figure 1.3b), and 0.19°C per decade (1958-2024, black line in Figure 1.3b), respectively. However, the annual temperature changes in other regions of Antarctica are less pronounced.

Extreme Event From July to August 2024, a rare persistent warming event occurred in Antarctica. This phenomenon initially emerged in Queen Maud Land and subsequently expanded across the entire Antarctic continent by August. During this period, the monthly average temperatures in most regions were more than 5°C above the climatic average (see Figures (a) and (b)). The Amundsen - Scott Station at the South Pole experienced 46 anomalously warm days from July to August, reaching the highest number of such days in the July-August period since 1957. Moreover, six stations in East Antarctica reported record-high average surface temperatures in August.

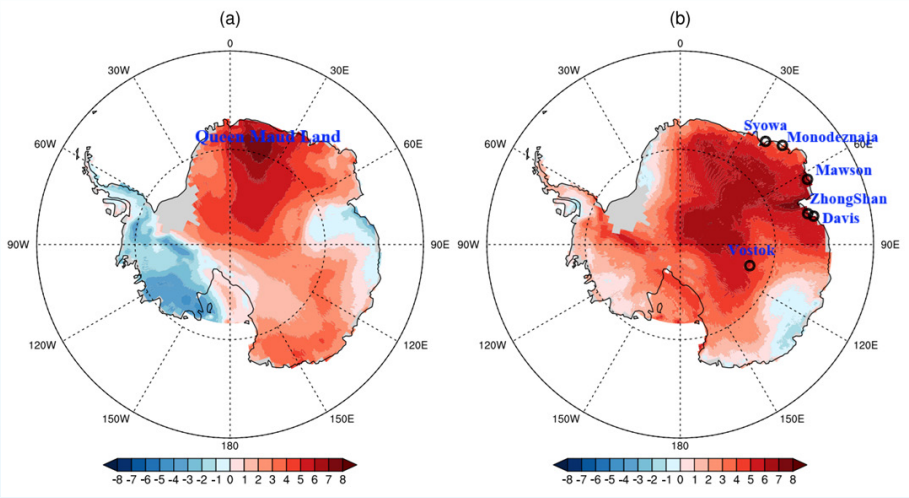

Figure Surface air temperature anomalies in Antarctic for (a)July and (b)August in 2024

In late July, a sudden stratospheric warming(SSW) event occurred in the Antarctic, disrupting the polar vortex. As a result, the cold air from the interior of Antarctica leaked out to the coastal areas, leading to the appearance of a rare “mother-of-pearl cloud,” that is, a rainbow-like polar stratospheric cloud, above Mawson Station.

Figure Stratospheric clouds photographed at Mawson Station in Antarctica between July 26 and 29, 2024
(From the news report on the website of the Australian Antarctic Program: https://www.antarctica.gov.au/news/2024/rare-iridescent-clouds-appear-over-mawson/)

1.1.2 Arctic

This subsection presents a systematic analysis of temperature changes in Arctic, based on the Global Historical Climatology Network (GHCN-D) and the Greenland weather observation dataset from the Danish Meteorological Institute, along with CMA-RA reanalysis data. All data have undergone rigorous quality control. The results indicate that the annual temperature over the Arctic in 2024 was -6.89°C, which is 0.65°C higher than the long-term average. Regarding seasonal distribution, the average temperatures during boreal winter (December to February), spring (March to May), summer (June to August), and autumn (September to November) were -19.37°C, -10.33°C, 6.51°C, and -4.99°C, respectively. Notably, in 2024, the Arctic exhibited warm anomalies during the winter, summer, and autumn months, with temperatures exceeding the long-term average by 0.51°C, 0.23°C, and 1.39°C, respectively. In contrast, spring recorded a cold anomaly, with temperatures 0.11°C below the long-term average.

The most apparent warming in 2024 occurred in the Canadian Arctic, where temperature increases exceeded 2°C (see Figure 1.4). Among the Arctic observation stations, the site with the greatest warming was Cambridge Bay, Canada, where the annual temperature was 3.30°C above the long-term average, setting a historical record (Figure 1.4-4). The annual temperatures for Cape Morris Jesup and Tromsø also reached historic highs (Figures 1.4-10 and 14), while Resolute and Holbæk reported the second highest annual temperatures on record (Figures 1.4-5 and 7). Of all the stations, only the U.S. station at Kotzebue and the Greenland station at Kangerlussuaq experienced cooler-than-average temperatures, with annual temperatures 0.05°C and 0.01°C below the long-term average, respectively (Figures 1.4-1 and 9).

Compared to 2023, there were slight variations in seasonal patterns. The warm anomalies during winter were primarily concentrated in the Canadian Arctic, with Holbæk reporting the largest winter warming in the entire Arctic, where winter temperatures were 4.88°C higher than the long-term average (Figure 1.4-7). In spring, the warm anomalies in the Canadian Arctic weakened somewhat, with Cambridge Bay exhibiting

the strongest spring warming in the Arctic, recording a temperature 3.54°C above the long-term average and setting a new historical record (Figure 1.4-4). Conversely, the West Siberian region experienced widespread cold anomalies, with Novy Port reporting the greatest temperature drop in the Arctic during spring, with temperatures 2.33°C below the long-term average (Figure 1.4-17). In summer, northern Europe displayed pronounced warm anomalies, with stations in Barentsburg, Tromsø, Lake Lovozero, and Hatanga recording temperatures exceeding the long-term average by 2.52°C, 3.03°C, 2.96°C, and 2.74°C, respectively (Figures 1.4-13, 14, 15, and 20), achieving historical highs. In autumn, apparent warm anomalies appeared in the Canadian Arctic and northern Greenland, with temperatures in Cambridge Bay, Resolute, Eureka, Holbæk, Thule, and Cape Morris Jesup exceeding the long-term average by more than 4°C, with Eureka experiencing an incredible increase of 5.92°C (Figures 1.4-4, 5, 6, 7, 8, and 10). Except for Holbæk, all these stations recorded their highest autumn temperatures on record, while Holbæk experienced the second highest autumn temperature. Additionally, northern Europe and West Siberia also exhibited strong warm anomalies, with

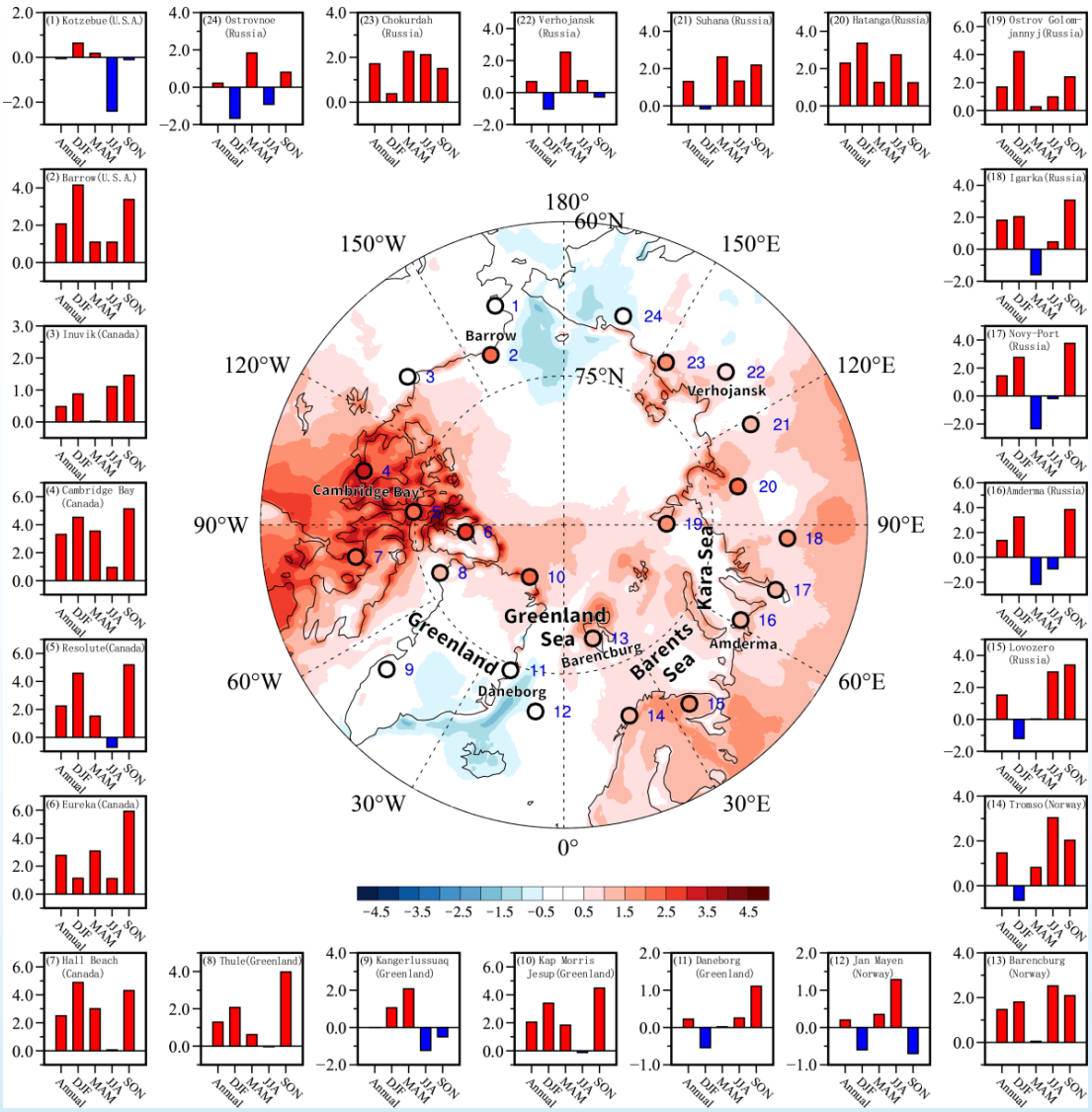

Figure 1.4 Spatial distribution of the 2024 annual mean temperature anomalies in Arctic and the annual and seasonal mean temperature anomalies at various stations (unit: °C)

both Lake Lovozero and Amderma recording their highest autumn temperatures on record (Figures 1.4-15 and 16), while Novy Port reported the second highest autumn temperature (Figure 1.4-17).

In the context of global warming, the annual temperature over the Arctic has exhibited a rapid increasing trend between 1979 and 2024 (see Figure 1.5), with a rate of 0.52°C per decade. This rate is 2.9 times higher than the global average warming rate, indicating the Arctic's high sensitivity to global changes. Furthermore, the significant warming in the Arctic is evident across different seasons, with particularly pronounced warming rates in autumn and winter, at 0.74°C per decade and 0.54°C per decade, respectively. In contrast, the warming during summer is relatively modest, at 0.33°C per decade.

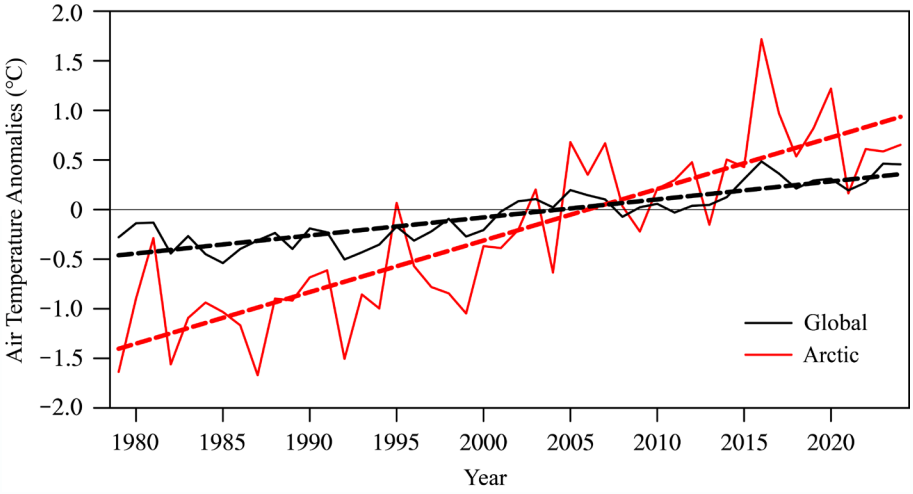

Figure 1.5 Time series of annual mean surface temperature anomalies averaged over Arctic (solid red line) and globally (solid black line) from 1979 to 2024, along with their trends (dashed lines) (unit: °C)

The rapid warming in the Arctic is particularly pronounced in the Arctic Ocean region, while the warming rate on land, although somewhat slower, remains significantly higher than the global average. All observation stations in the Arctic have shown a clear warming trend since records began, with an acceleration of this warming rate starting in the 1980s (see Figure 1.6). From 1981 to 2024, Barrow Station in Alaska recorded the fastest warming rate, increasing by 1.08°C per decade. This was followed closely by Barentsburg and Amderma stations along the Barents and Kara Seas, which recorded warming rates of 0.98°C and 0.88°C per decade, respectively. In contrast, the warming rates at Cambridge Bay, Verkhoyansk, and Daneborg were slightly lower, with increases of 0.65°C, 0.51°C, and 0.44°C per decade, respectively.

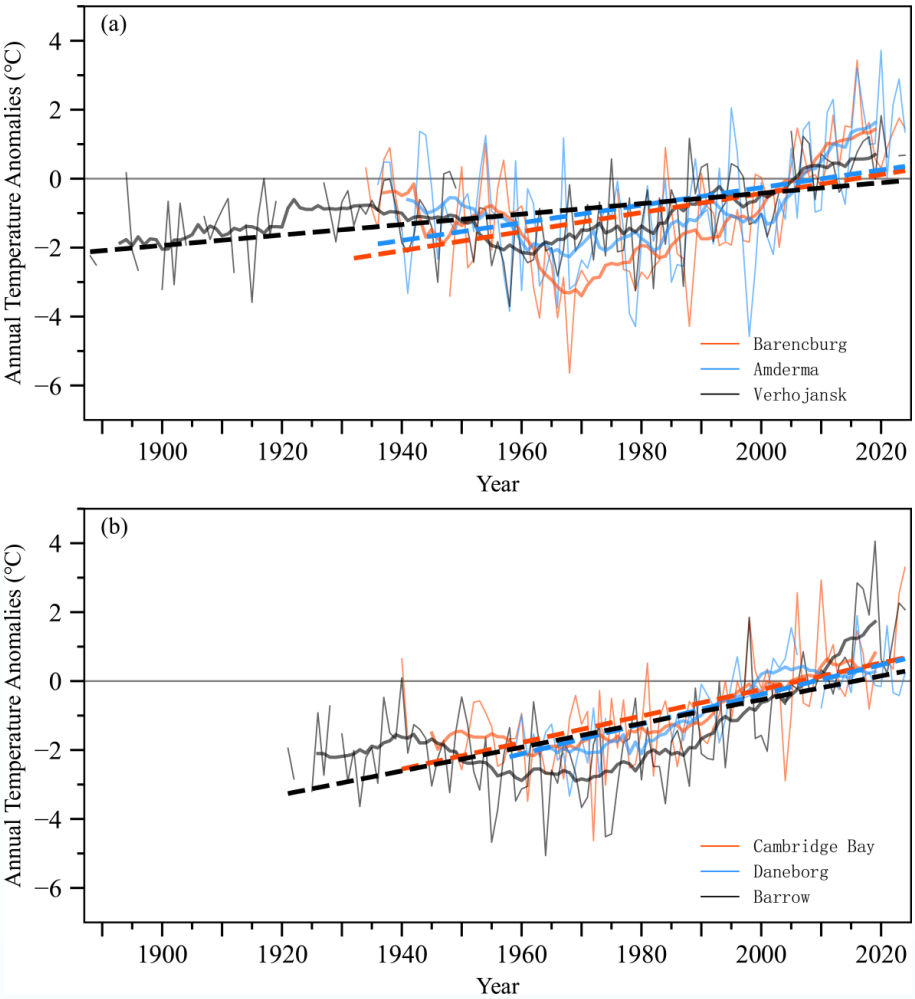

Figure 1.6 Time series of annual mean temperature anomalies at warming sites in the Arctic regions of Eurasia (a) and North America (b). The thin solid line represents the annual mean temperature anomalies, the thick solid line represents the 11-year running average of annual mean temperature anomalies, and the dashed line indicates the trend in annual mean temperature anomalies

Extreme Events The summer of 2024 was the third hottest on record in the Arctic region. Multiple stations in Alaska and the Arctic regions of Canada set new highs for daily maximum temperatures. For example, the temperature at Deadhorse station reached 31.7℃ on August 6th, and the temperature at Inuvik station reached 34.8℃ on August 7th. The summer of 2024 was the wettest summer ever in the Arctic, and the summer precipitation in the area north of 60°N set a new historical record.

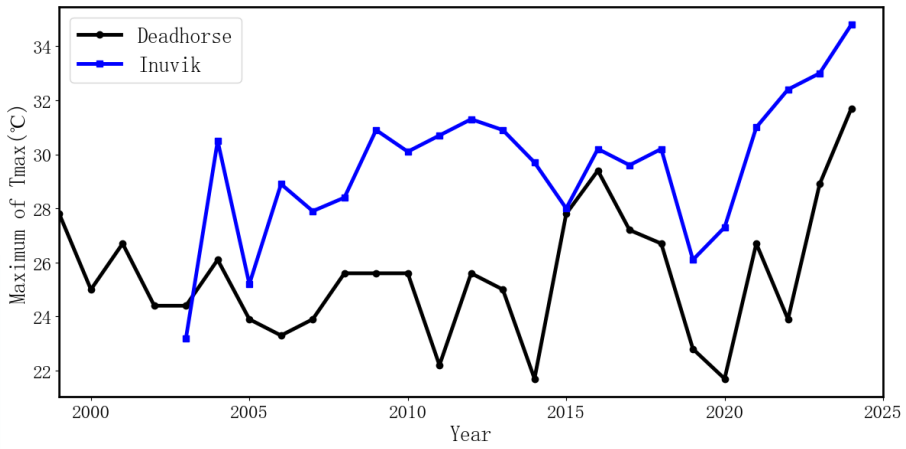

Figure Annual maximum of daily maximum temperature(Tmax) for the station of Deadhorse(1999–2024) and Inuvik(2003–2024)

1.2 Sea Surface Temperature

This section utilizes the Operational Sea Surface Temperature and Sea Ice Analysis (OSTIA) dataset, a global high-resolution sea surface temperature (SST) and sea ice cover product released by the UK Met Office. We analyze SST anomalies using the 1991–2020 climatological mean as the baseline.

1.2.1 Southern Ocean

In March 2024, the sea ice along the Antarctic continental margins was nearly fully depleted, with residual ice persisting only in partial areas of the Weddell and Ross Seas. Compared to the climatological average, Southern Ocean SST anomalies were predominantly concentrated in the Pacific sector: cold anomalies dominated the southwestern Pacific (180°–120°E) and southeastern Pacific (120°W–60°W), while warm anomalies prevailed in the central Pacific (120°W–180°), collectively forming a distinct dipole pattern. Relative to March 2023, the Pacific sector SST anomalies in 2024 maintained a similar dipole structure, characterized by cold anomalies in the eastern and western regions and warm anomalies in the central zone, but with enhanced intensity and broader spatial coverage. Notably, the cold anomaly in the southeastern Pacific extended northeastward into the Atlantic sector, whereas the Indian Ocean sector exhibited overall warming trends.

In September 2024, the Southern Ocean sea ice extent expanded to near 60°S. Except for the southwestern Atlantic Ocean, SST near the sea ice edge exhibited overall warm anomalies compared to the climatological average. Relative to September 2023, the SST distribution in September 2024 displayed a dipole pattern

similar to that of March: cold anomalies dominated the Atlantic sector and southwestern Pacific, whereas warm anomalies prevailed in other regions.

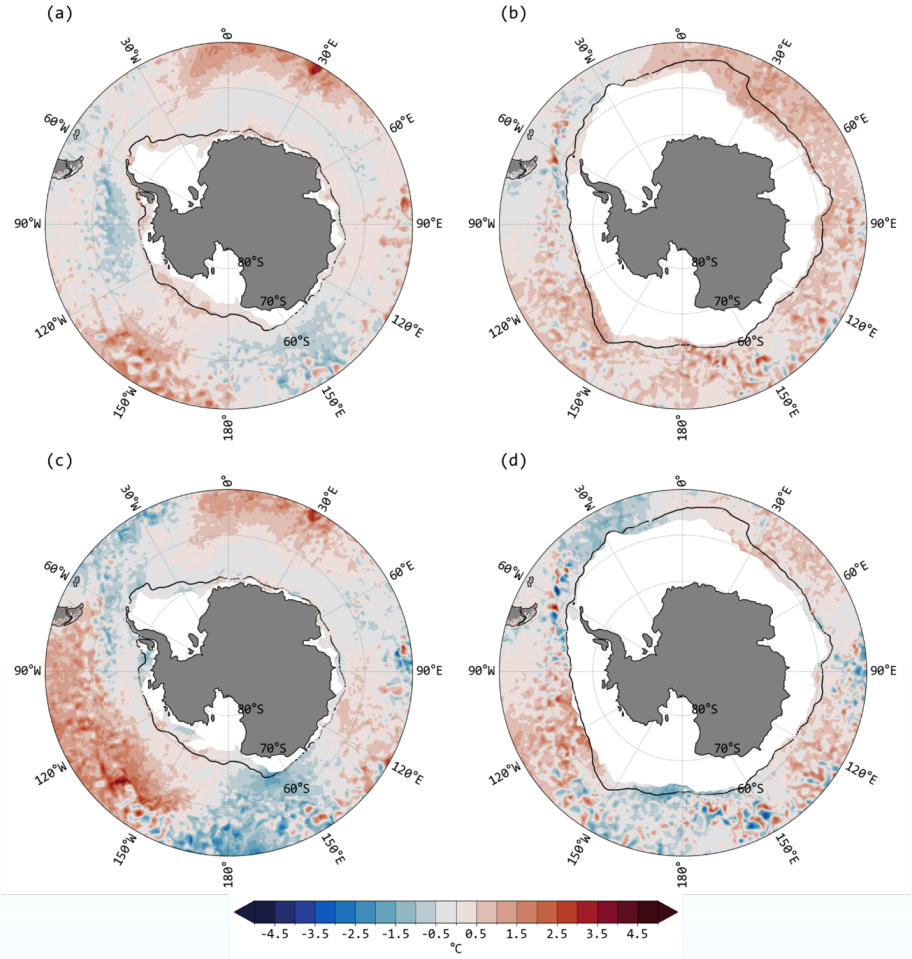

Figure 1.7 SST Anomaly Distribution in the Southern Ocean, March and September 2024
(a) Sea Surface Temperature Anomaly (SST Anomaly) in the Southern Ocean, March 2024 (Unit: ℃); (b) SST Anomaly in the Southern Ocean, September 2024 (Unit: ℃); (c) SST Anomaly in the Southern Ocean, March 2024 Relative to March 2023 (Unit: ℃); (d) SST Anomaly in the Southern Ocean, September 2024 Relative to September 2023 (Unit: ℃). In all panels, white areas and black solid lines indicate the climatological mean sea ice extent and marginal ice zone position for the respective months, respectively

1.2.2 Arctic Ocean

In March 2024, sea ice coverage was extensive across the Arctic Ocean. Limited open water persisted only in regions influenced by the North Atlantic Current, including the Norwegian Sea, Barents Sea, and near the Svalbard archipelago. Overall Arctic SST remained low, with most areas approaching the seawater freezing point. Compared to the climatological mean, however, the Arctic Ocean exhibited basin-wide warm anomalies during March 2024. Relative to the same period in 2023, Arctic SST anomalies displayed regional disparities: the Norwegian Sea experienced warm anomalies, while the Barents Sea was dominated by cold anomalies.

In September 2024, Arctic SST anomalies were predominantly warm relative to the climatological mean,

with cold anomalies confined to the Chukchi Sea and coastal areas south of Greenland. Notably, the cold anomaly in the Chukchi Sea extended southward into the Bering Sea. Compared to September 2023, SSTs in September 2024 were generally lower, with pronounced regional heterogeneity in anomaly distribution: warm anomalies were concentrated in the northern Laptev Sea, northern Beaufort Sea, and Barents Sea, whereas cold anomalies prevailed in the Chukchi Sea, Bering Sea, southern Beaufort Sea, and Kara Sea.

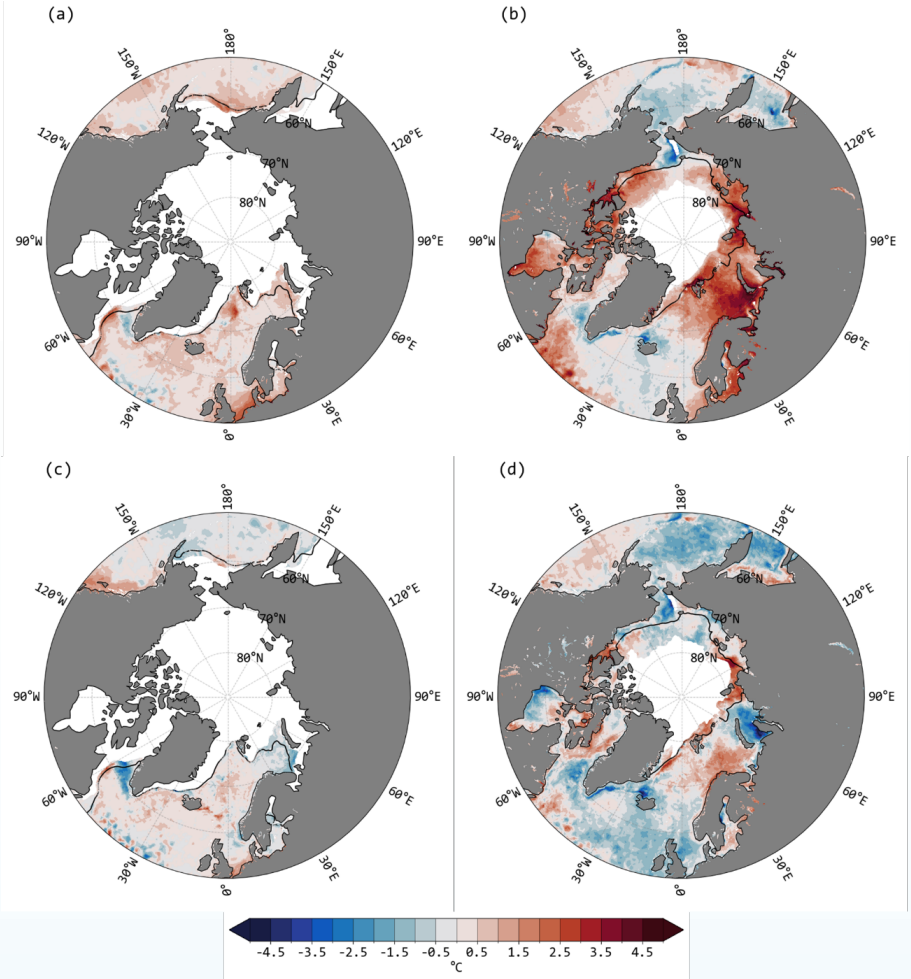

Figure 1.8 Arctic Ocean SST Anomaly Distribution, March and September 2024
(a) Sea Surface Temperature Anomaly (SST Anomaly) in the Arctic Ocean, March 2024 (Unit: ℃); (b) SST Anomaly in the Arctic Ocean, September 2024 (Unit: ℃); (c) SST Anomaly in the Arctic Ocean, March 2024 Relative to March 2023 (Unit: ℃); (d) SST Anomaly in the Arctic Ocean, September 2024 Relative to September 2023 (Unit: ℃). In all panels, white areas and black solid lines denote the climatological mean sea ice extent and marginal ice edge position for the corresponding months, respectively

Extreme Events In August 2024, the pan-Arctic Ocean's average sea surface temperature (SST) was approximately 0.6°C above the climatological mean, yet anomalous spatial heterogeneity dominated across marginal seas. The Barents Sea recorded its highest monthly SST in observational history, nearly 3°C above the climatological mean, while the Chukchi Sea—observed to be cooling persistently in recent years—registered its lowest August SST on record, over 2°C below the climatological mean. (Source: Arctic Report Card 2024).

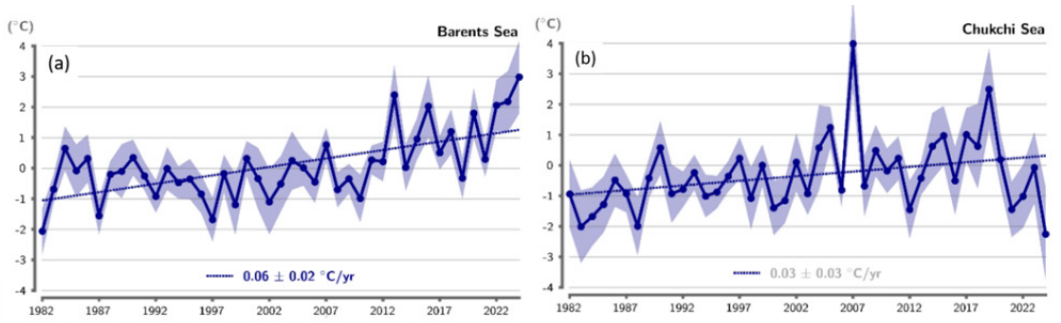

Figure Spatially Averaged August Sea Surface Temperature (SST) Anomalies (Unit: °C) Across Regions Relative to the 1991–2020 August Mean, 1982–2024, (a) Barents Sea; (b) Chukchi Sea. Dashed lines indicate linear trends in SST anomalies from 1982 to 2024, with trend values (in °C/year) annotated in the legend, including 95% confidence intervals. Trends lacking statistical significance ($p \geqslant 0.05$) are shaded in gray. Blue-shaded regions denote the ±1 standard deviation range of the regional mean SST anomalies. (Source: Adapted from Arctic Report Card 2024).

1.3 Air Pressure

Changes in the air pressure field are one of the key linkages between the polar regions and the global climate system. This section analyzes the spatial anomaly characteristics of the air pressure fields in the Arctic and Antarctic in 2024, as well as important circulation phenomenons such as the polar vortex and atmospheric oscillations. The Arctic polar vortex index is sourced from the National Climate Center, and the oscillation indices are calculated based on the CMA-RA reanalysis dataset.

1.3.1 Antarctic

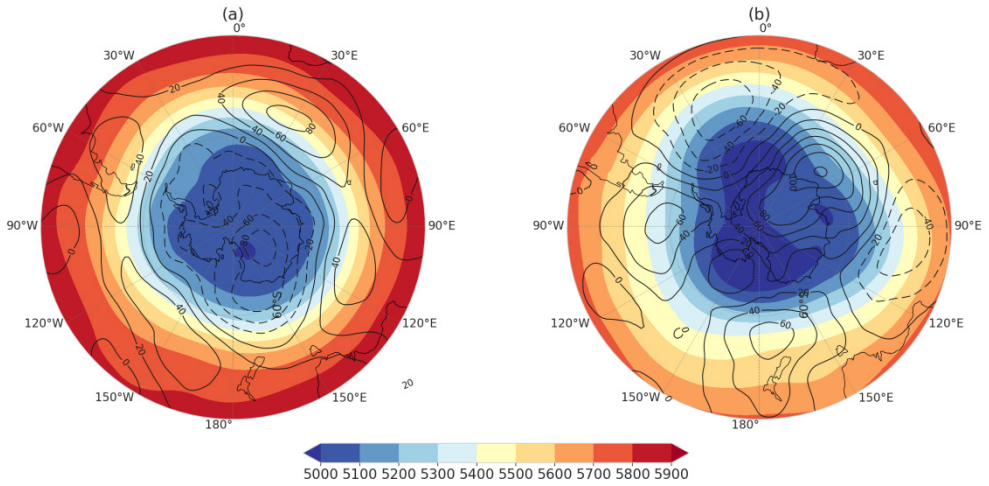

Figure 1.9 The 500 hPa geopotential height field (color map) and its anomaly field (contour map) for the Antarctic in 2024 during (a) summer (December–February) and (b) winter (June–August). Units: geopotential meters(gpm)

In the summer of 2024, the 500 hPa geopotential height field over the Antarctic continent was dominated by negative anomalies (Figure 1.9), with multiple positive anomaly centers encircling Antarctica, characteristic of a typical positive phase of the Antarctic Oscillation (AAO). In winter, the 500 hPa geopotential height field over the Antarctic continent was dominated by positive anomalies, exhibiting an approximately three-wave pattern around the continent. Among these, the positive geopotential height anomaly over East Antarctica was the strongest and most extensive, covering the majority of the Antarctic continent. Meanwhile, the negative anomalies near the Weddell Sea was also relatively strong, whereas the anomalies near the Ross Ice Shelf was weaker.

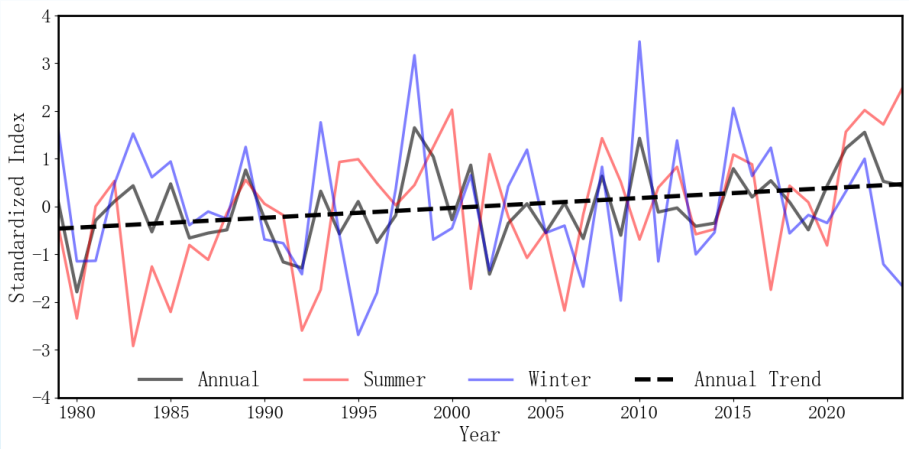

Figure 1.10 The standardized AAO index for the time period of 1979–2024

In 2023, the standardized Antarctic Oscillation(AAO) Index exhibited a strong negative value in winter and a strong positive value in summer, and such seasonal contrast had further intensified in 2024(Figure 1.10). The summer AAO index reached a record high of 2.47, the highest value since 1979, while the winter index dropped to -1.66, ranking as the fifth lowest value since 1979. For the AAO, both the positive phase in summer and the negative phase in winter strengthened significantly in 2024.

1.3.2 Arctic

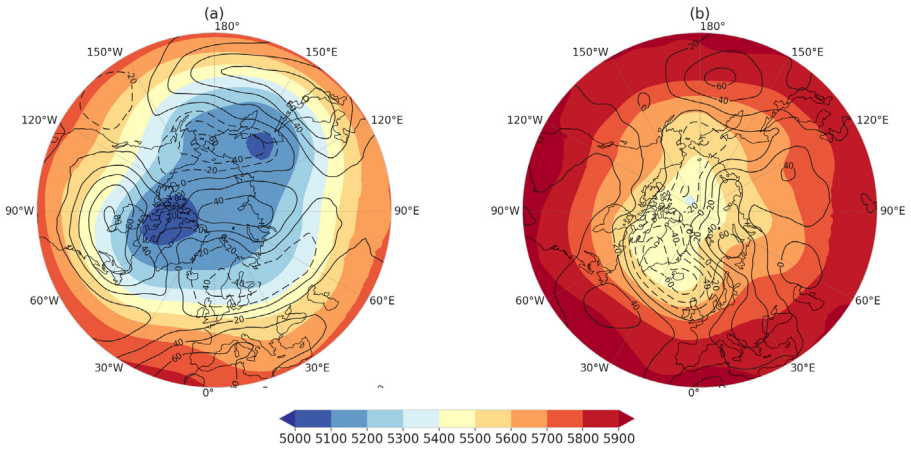

Figure 1.11 The 500 hPa geopotential height field (color map) and its anomaly field (contour map) for the Arctic in 2024 during (a) winter (December–February) and (b) summer (June–August). Units: gpm

As indicated in Figure 1.11, during the boreal winter of 2024, the 500 hPa geopotential height field over the Arctic exhibited a pattern of negative-positive-negative anomalies stretching from the North Atlantic to the Bering Strait. The positive anomalies was located near the North Pole, implying a weak low pressure over

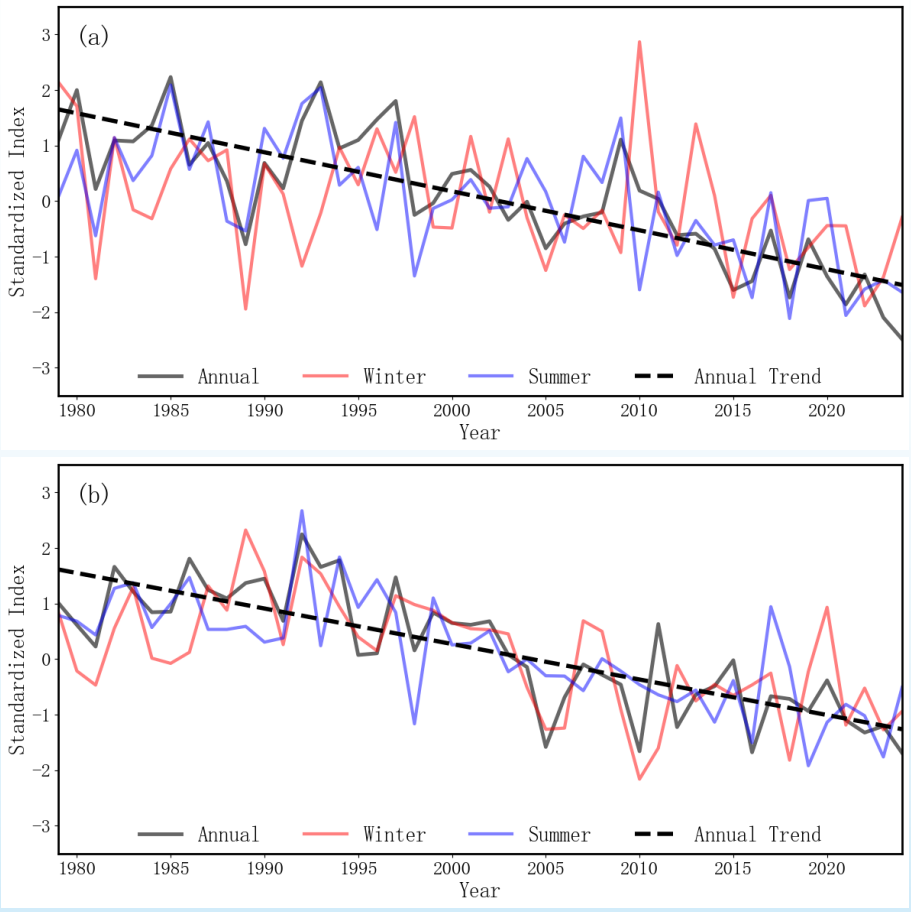

Figure 1.12 The standardized index for (a) Arctic vortex area and (b) Arctic vortex intensity during 1979–2024

the Arctic center. In the boreal summer, negative anomalies in the 500hPa geopotential height field dominated most of the Arctic Ocean, with the center located near Iceland. However, positive anomalies were observed on the Eurasian continent side.

As shown in Figure 1.12, in 2024, the standardized index of the Arctic vortex area was -0.292 in winter, -1.640 in summer, and -2.487 on an annual average. Compared to 2023, the winter value increased significantly, the summer value showed little change, and the annual average index set a new record low, following the previous low of -2.096 in 2023. For the standardized index of the Arctic vortex intensity, the values were -0.941 in winter, -0.508 in summer, and -1.691 on an annual average in 2024. Compared to 2023, both winter and summer values increased slightly, while the annual average index decreased by 0.485 from the 2023 value of -1.206, marking a new record low since 1979. However, this new low is not significantly different from the previous lows recorded in 2010 and 2016. Notably, the changes in the Arctic vortex area and intensity in 2024, whether in winter, summer, or on an annual basis, did not alter the overall negative trend in the Arctic vortex area and intensity indices since 1979.

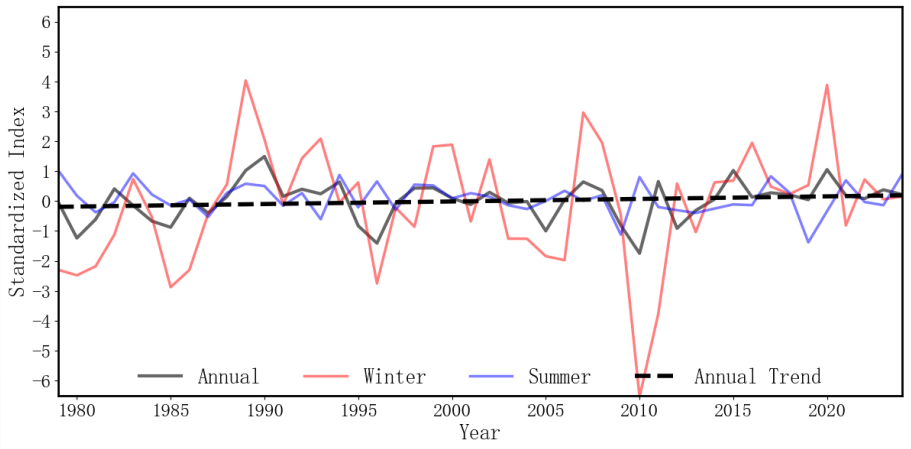

Figure 1.13 The standardized Arctic Oscillation(AO) index for the time period of 1979–2024

In 2024, the standardized Arctic Oscillation Index (Figure 1.13) was 0.15 in winter, 0.89 in summer, and 0.22 on an annual average. Notably, the summer value exhibited a relatively strong positive anomaly.

Chapter 2 Sea Ice

The data used in this chapter are the sea ice extent (SIE) products from the National Snow and Ice Data Center (NSIDC) of the United States for the period from 1979 to 2024. The climatology is defined as the average from 1991 to 2020. In addition, the sea ice concentration products based on China's Fengyun series satellites provided by Sun Yat-sen University, as well as the sea ice melting/freezing time datasets provided by the National Aeronautics and Space Administration (NASA) of the United States and Ocean University of China (OUC) are also used.

2.1 Sea Ice Extent

2.1.1 Antarctic

The Antarctic SIE shows obvious seasonal variability (Figure 2.1a). The freezing period usually spans from March to September, and the melting period spans from October to February of the following year. The minimum SIE throughout the year usually occurs from the end of February to the beginning of March. On February 20, 2024, the Antarctic SIE reached its lowest record, with a total area of 1.97×10^6 km², next only to the lowest records in 2022 (on February 25, 1.96×10^6 km²) and 2023 (on February 21, 1.77×10^6 km²), ranking as the third lowest value. The annual maximum SIE in Antarctica in 2024 (17.18×10^6 km²) is second only to that in 2023 (16.99×10^6 km²), being the second lowest value in history. Generally speaking, the Antarctic SIE in 2024 was unusually low, and the annual average SIE was second to that in 2023, ranking as the second lowest value. It is worth mentioning that the SIE in Antarctica in November (14.19×10^6 km²) sets the lowest record for this month over the past 46 years. In terms of the change trend, the Antarctic SIE showed a trend of first slowly increasing and then rapidly decreasing during the period from 1979 to 2024 (Figure 2.1b).

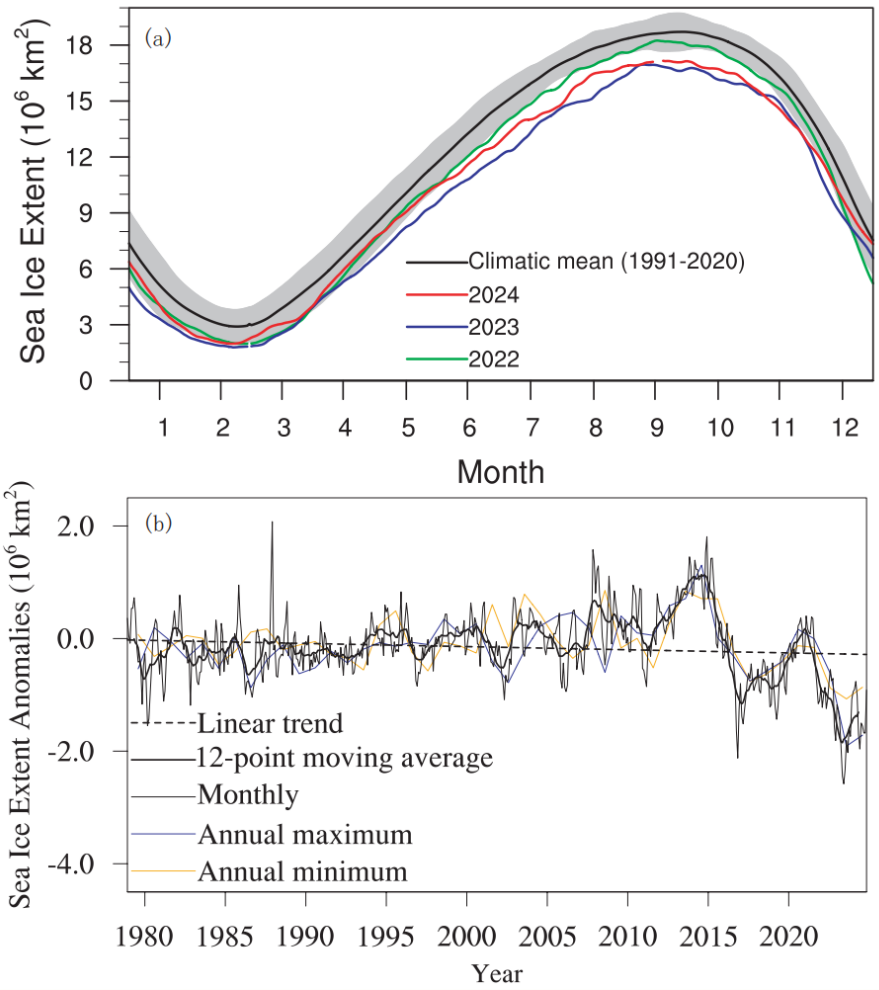

Figure 2.1 (a) Antarctic climatic SIE, along with ±2 standard deviations (gray shaded area), and the monthly SIE in 2022, 2023, and 2024; (b) The time series of Antarctic monthly SIE anomalies (thin black line) and its 12−point moving average (thick black solid line), linear trend (dashed line), and the annual minimum SIE (orange), the annual maximum SIE (blue) from 1979 to 2024 (unit: 10^6 km^2)

2.1.2 Arctic

The Arctic SIE also exhibits obvious seasonal variability (Figure 2.2a). The freezing period of Arctic sea ice spans from late September to March of the following year, and the melting period spans from April to mid-September. The minimum SIE throughout the year usually occurs in mid-September. The annual lowest record of Arctic SIE in 2024 was 4.21×10^6 km², which was comparable to that in 2023, ranking as the seventh lowest value. It is worth noting that the Arctic SIE in December 2024 (11.42×10^6 km²) sets the lowest record for this month over the past 46 years. In terms of the change trend (Figure 2.2b), since 1979, the Arctic SIE has generally decreased at a rate of 5.12×10^5 km² per decade. Moreover, the downward trend of the annual minimum extent is 7.81×10^5 km² /10a, and the downward trend of the annual maximum extent is 3.92×10^5 km² /10a. In recent years, the decreasing trend of the annual average SIE has slowed down to some extent.

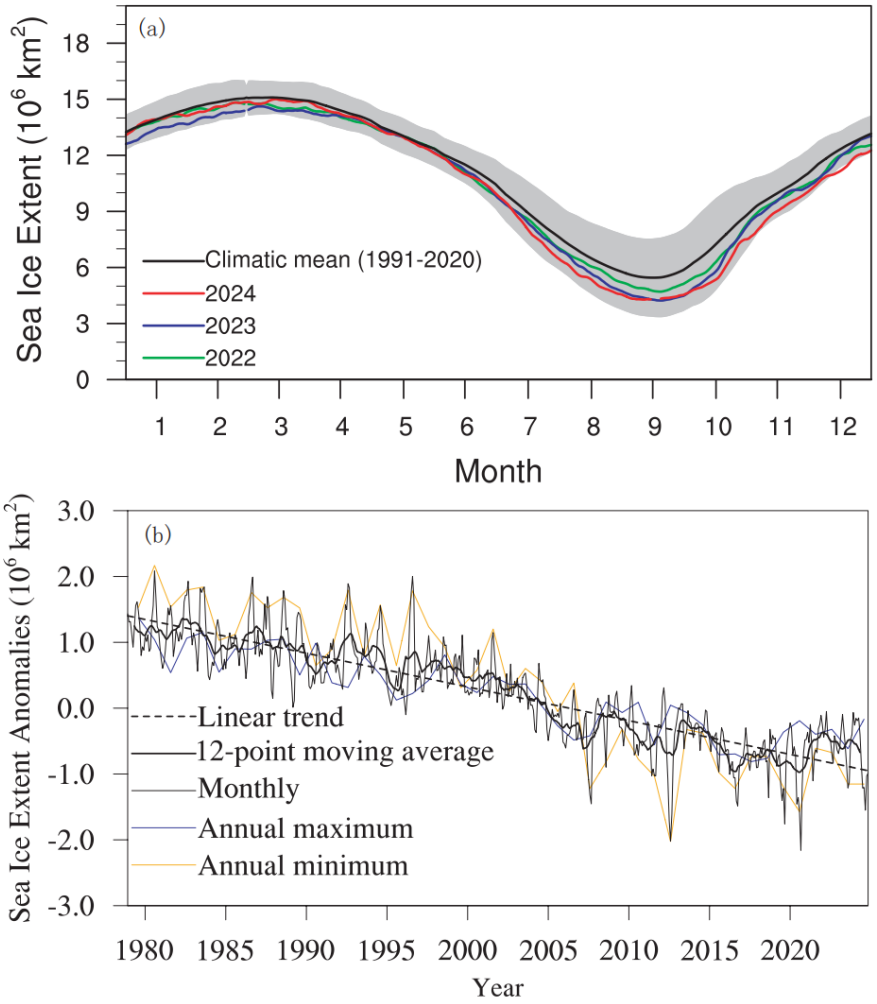

Figure 2.2 (a) Arctic climatic SIE, along with ±2 standard deviations (gray shaded area), and the monthly SIE in 2022, 2023, and 2024; (b) The time series of Arctic monthly SIE anomalies (thin black line) and its 12−point moving average (thick black solid line), linear trend (dashed line), and the annual minimum SIE (orange), the annual maximum SIE (blue) from 1979 to 2024 (unit: 10^6 km^2)

2.2 Sea ice concentration

2.2.1 Antarctica

Figure 2.3 shows the monthly mean and anomalies (relative to 2012-2024) of the sea ice concentration (SIC) in the Antarctica for February and September in 2024. In February, the SIC was lower than the average for February during 2012-2024. Sea ice was primarily distributed in the Weddell Sea, Amundsen Sea, and along the coast of Victoria Land, where multi-year sea ice predominantly occurs. Except for the eastern Weddell Sea and coastal areas of Victoria Land where the SIC was higher than the multi-year average, the SIC in other regions was generally lower, particularly in the Bellinghausen Sea, which was largely below the average.

In September, sea ice essentially encircles the Antarctic continent, with areas of decreased SIC being

larger than those with increased SIC. There is an increasing trend of SIC in the Bellinghausen Sea and the eastern Weddell Sea, while the western Weddell Sea, Ross Sea, and Amundsen Sea experienced a decrease trend. In the western Indian Ocean, the SIC notably decreased, while in the eastern Indian Ocean and the Pacific Ocean, the SIC showed more complex changes without a uniform changing trend.

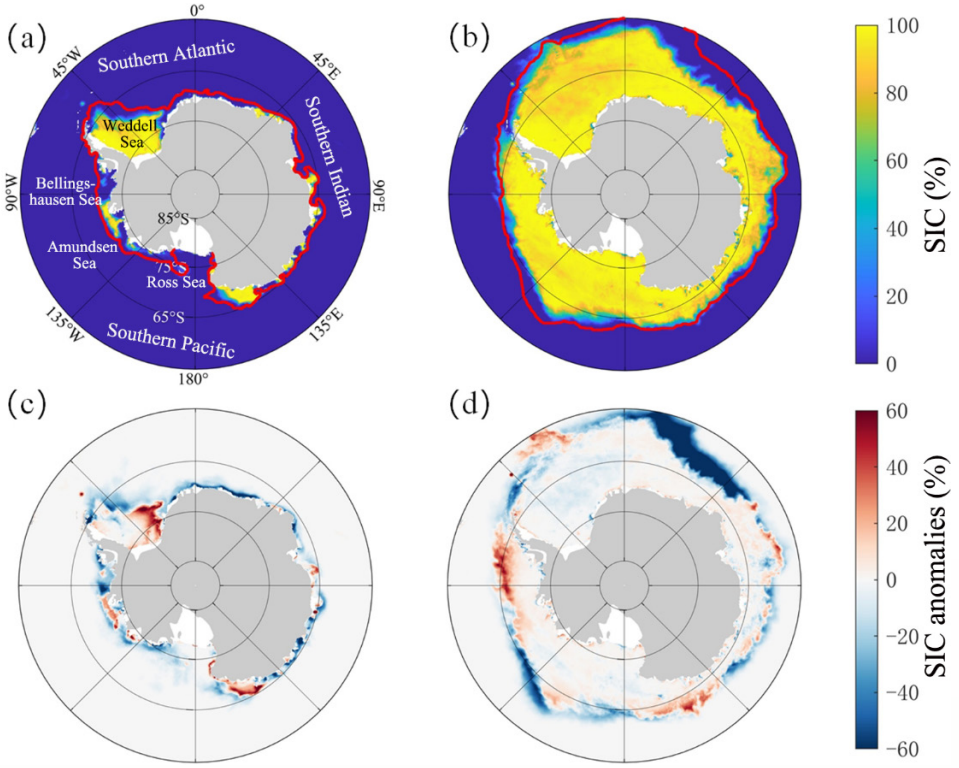

Figure 2.3 the SIC and its anomalies (relative to 2012–2024, unit: %) in the Antarctica for 2024 based on the Fengyun series meteorological satellite imagery. (a) the SIC in February; (b) the SIC in September; (c) the SIC anomalies in February; (d) the SIC anomalies in September. The red solid line indicates the average sea ice extent during 2012–2024

2.2.2 Arctic

Figure 2.4 shows the monthly mean and anomalies (relative to 2012-2024) of the SIC in the Arctic for March and September in 2024. In March, the SIC in the central Arctic Ocean was similar as the multi-year average during 2012-2024, with large anomalies observed only in the marginal zones. In the Greenland Sea and Barents Sea, the SIC in the marginal zones increased, while the SIC in the Bering Sea showed more complex changes, namely it increased in the northern part and decreased in the southern part. In September, the areas with decreased SIC were mainly distributed in the Beaufort Sea, the Canadian Archipelago, the Greenland Sea and the Barents Sea. Areas with increased SIC were primarily located in the high-latitude regions of the Laptev Sea, the East Siberian Sea and the Chukchi Sea. The SIC notably increased to the east of Wrangel Island in the East Siberian Sea.

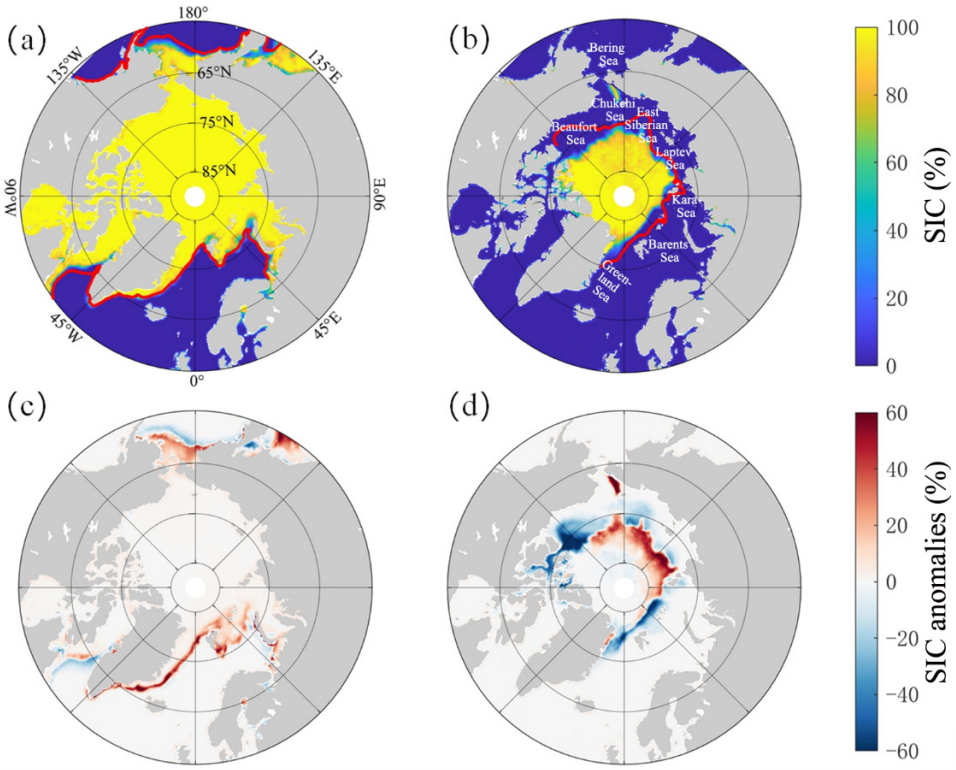

Figure 2.4 the SIC and its anomalies (relative to 2012–2024, unit: %) in the Arctic for 2024 based on the Fengyun series meteorological satellite imagery. (a) the SIC in March; (b) the SIC in September; (c) the SIC anomalies in March; (d) the SIC anomalies in September. The red solid line indicates the average sea ice extent during 2012–2024

2.3 Sea Ice Melt Season

The onset of sea ice melt and freeze marks the beginning and end of the sea ice melt season. The melt onset (MO) is defined as the first day of continuous sea ice melting during summer, while the freeze onset (FO) is the first day when new ice begins to form in open water and the bare or lightly snow-covered ice surface undergoes continuous refreezing. The number of days between the MO and FO is the sea ice melt season length.

The Arctic sea ice surface MO spans from late March in the ice-margin areas to June in the central Arctic (Fig. 2.5a). Compared to the 2011-2024 average, the 2024 MO anomalies show a spatial inconsistency, with early MO in the central Arctic, the Sea of Okhotsk, and southern Hudson Bay, and late MO in the marginal areas of the Beaufort, Chukchi, Kara, Bering and Baffin Bays (Fig. 2.5c). In 2024, the mean date of MO in the regions north of 70°N was recorded as the 156th day, which is merely 0.7 days earlier than the average observed over the period from 2011 to 2024. The SMMR-SSM/I-SSMIS data published by NASA indicate that the MO in the Arctic exhibited an advancing trend from 1979 to 2022, with a rate of -1.47 d per decade. However, during the operational period of the FY-3B/3D satellites, both datasets revealed a delaying trend in the MO. Specifically, the MWRI data from 2011 to 2024 demonstrate that the MO was delayed at a rate of 4.2 d per decade (Fig. 2.6a).

The Arctic sea ice surface FO spans from August in the central Arctic to January of the following year

in the marginal sea ice region (Fig. 2.5b). The FO in 2024 also shows spatial inconsistency compared to the average conditions in 2011-2024. The FO occurred early in the multiyear ice margins of the Laptev and East Siberian Seas, and in the Chukchi Sea. Notably, in the summer ice marginal areas of the Laptev Sea, the FO was approximately 15 days earlier than the multiyear average, consistent with regions displaying significant positive anomalies in September sea ice concentration (Fig. 2.4). In the central Arctic, the spatial distribution of regions with earlier and later FO in 2024 is discontinuous. In the remaining regions, the FO is predominantly delayed. In 2024, the average FO in regions north of 70°N was recorded as the 285.5th day, which is 7.4 days later than the average from 2011 to 2024. Data from the FY-3B/3D satellites show that during the period from 2011 to 2024, the FO exhibited a delaying trend at a rate of 2.9 d per decade (Fig. 2.6b).

The length of the sea ice melt season in the Arctic north of 70°N shows a lengthening trend in 1979-2022, with a rate of 6.3 d per decade. However, from 2011 to 2024, a slight shortening trend was observed, with a rate of 0.7 d per decade (Fig. 2.6c). This shift is primarily attributed to the fact that both MO and FO are delayed in this time period, and the rate of change in MO is greater than that in FO.

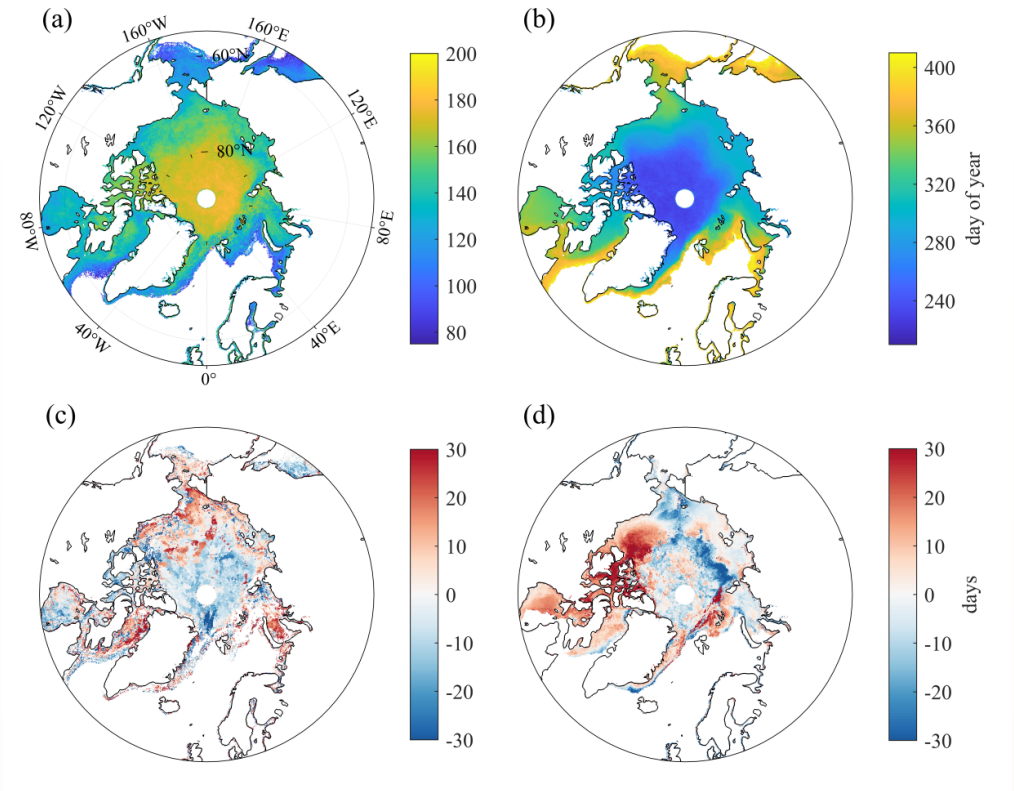

Figure 2.5 (a) Melt onset and (b) Freeze onset as averaged from 2011 to 2024. (c) Melt onset and (d) Freeze onset anomalies of 2024

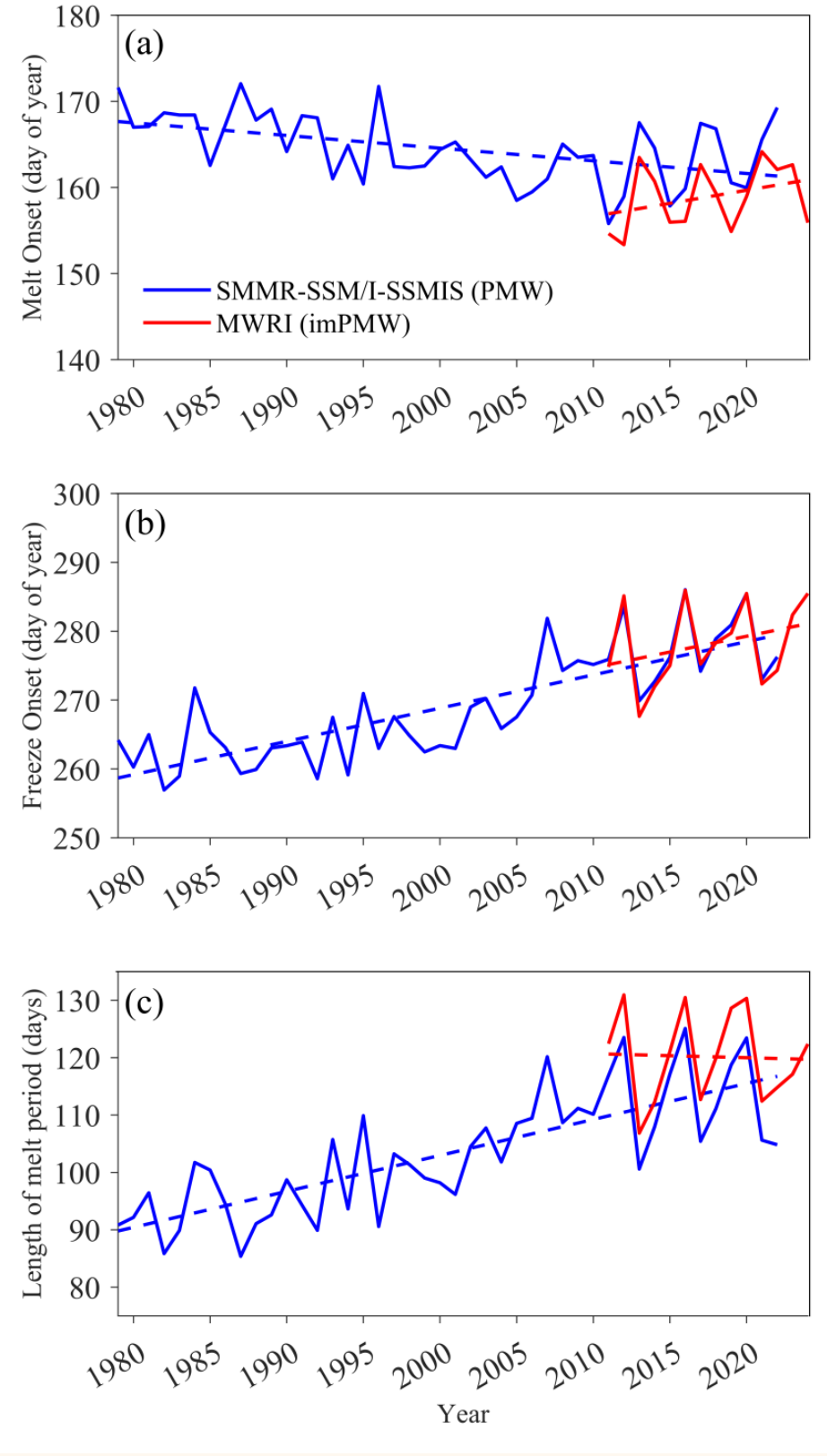

Figure 2.6 Time series of annual averages north of 70°N of (a) the melt onset, (b) the freeze onset, and (c) the melt season length for data from NASA (blue) and OUC (red)

Chapter 3 Atmospheric Composition

3.1 Major Greenhouse Gases

Greenhouse gases refer to natural or anthropogenic gaseous components in the atmosphere that have the ability to absorb and emit longwave radiation from the Earth's surface, atmosphere, and clouds. This characteristic leads to the greenhouse effect. According to the Kyoto Protocol, the major greenhouse gases in the Earth's atmosphere include carbon dioxide (CO_2), methane (CH_4), nitrous oxide (N_2O), as well as sulfur hexafluoride (SF_6), hydrofluorocarbons (HFCs), and perfluorocarbons (PFCs).This section is based on data collected at polar stations from the World Data Centre for Greenhouse Gases (WDCGG) and China's Zhongshan Station. There are 13 stations in Antarctica and 16 stations in the Arctic (Figure 3.1), covering the period from 1984 to 2023 (the concentrations of these greenhouse gases have currently only been published up to 2023). This section mainly analyzes the variations of four major greenhouse gases: carbon dioxide, methane, nitrous oxide, and sulfur hexafluoride.

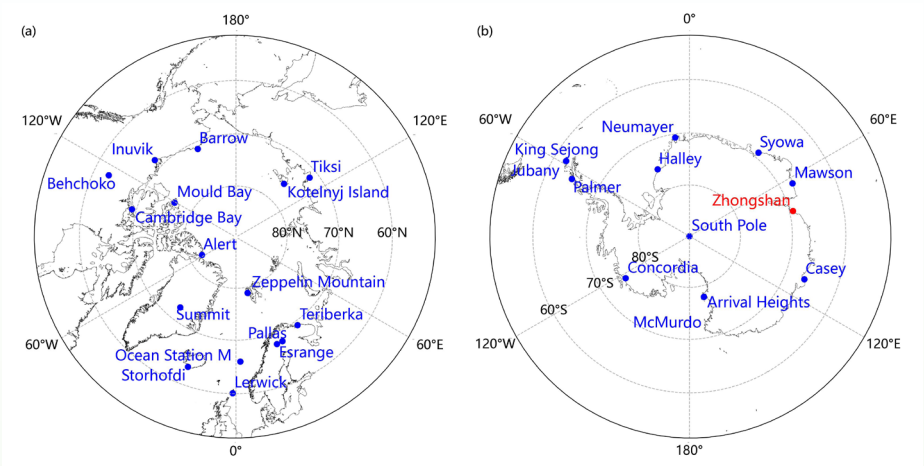

Figure 3.1 Locations of major polar atmospheric composition observation stations

3.1.1 Antarctica

(1) CO_2 and CH_4

From 1984 to 2023, the concentration of CO_2 in the Antarctic atmosphere showed a steady annual increase, with a growth rate of 1.88 ppm/year, which was generally consistent with the global trend (1.94 ppm/year) (Figure 3.2a). In 2023, the annual average concentration of CO_2 in the Antarctic atmosphere reached 416.39 ppm, which was 3.58 ppm lower than the global average. Compared to 2022, the annual average concentration increased by 1.99 ppm.

Similarly, the CH_4 concentration in the Antarctic atmosphere exhibited a stable upward trend, with a growth rate of 7.31 ppb/year, aligning with the global trend (7.14 ppb/year) (Figure 3.2b). In 2023, the annual average concentration of CH_4 in the Antarctic atmosphere reached 1870.60 ppb, which was 63.4 ppb lower

than the global average. Compared to 2022, the annual average concentration in Antarctica increased by 12.79 ppb.

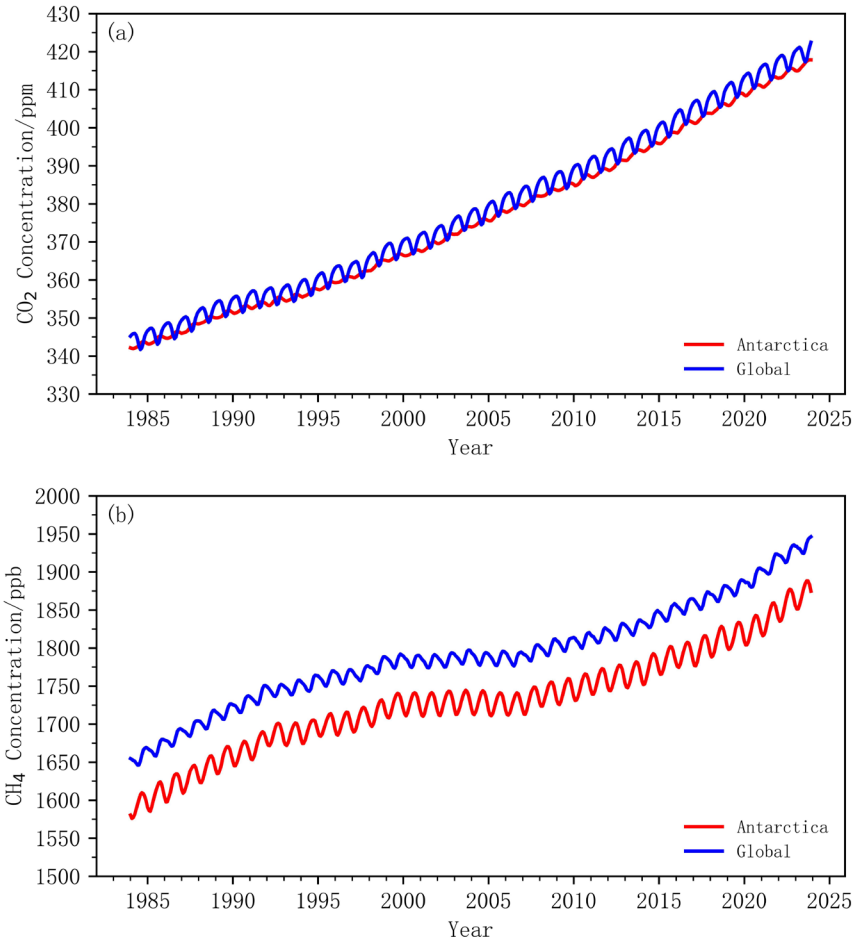

Figure 3.2 Changes in concentrations of CO_2 (a) and CH_4 (b) in Antarctica and the globe, 1984 to 2023

(2) N_2O and SF_6

According to observational data from six Antarctic stations monitoring N_2O concentrations,The annual average concentration of N_2O increased from 312.09 ppb in 1997 to 335.70 ppb in 2023, showing an average growth rate of 0.91 ppb/year across these stations (Figure 3.3a). The year 2023 alone saw a 1.20 ppb increase compared to 2022. China's Zhongshan Station, which initiated N_2O monitoring in 2008, demonstrates trends consistent with regional patterns. Between 2008 and 2023, the station recorded a concentration rise from 320.40 ppb to 335.14 ppb, equating to an annual growth rate of 0.98 ppb. Notably, 2023 witnessed a 1.15 ppb absolute increase (0.34% relative growth) in annual average N_2O concentrations at Zhongshan Station compared to 2022.

From 1997 to 2023, all three Antarctic stations monitoring SF_6 showed a significant increasing trend in annual average concentrations (Figure 3.3b). The annual average concentration increased from 3.83 ppt in 1997 to 11.15 ppt in 2023. The concentration increased 2.9 times in 27 years with an average growth rate of 0.28 ppt/year. In 2023, the annual average concentration of SF_6 at the three Antarctic stations increased 0.37 ppt compared to 2022, but slightly lower than the increase in 2021-2022.

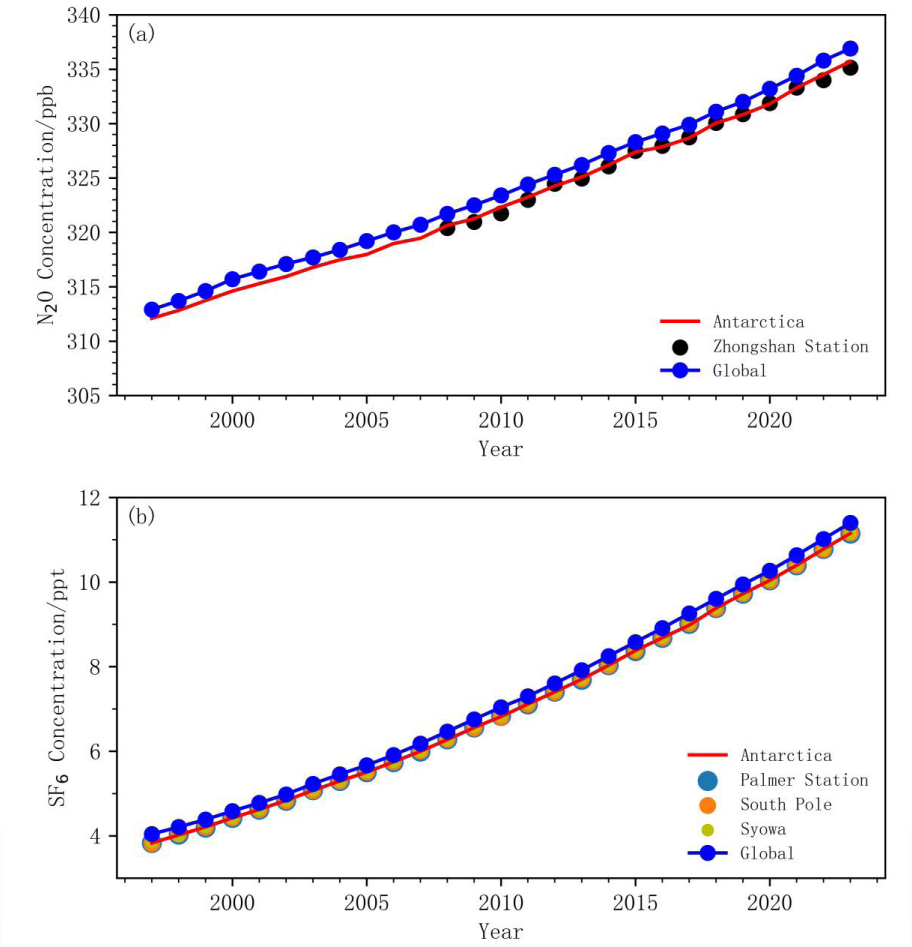

Figure 3.3 Annual average concentrations of (a) N_2O and (b) SF_6 (1997 – 2023) in Antarctica
Note: the global average concentration of SF_6 is from NOAA

3.1.2 Arctic

(1) CO_2 and CH_4

From 1984 to 2023, the concentration of CO_2 in the Arctic atmosphere exhibited a steady annual increase, generally consistent with the global average trend (Figure 3.4a), with an average growth rate of 1.95 ppm/year. In 2023, the annual average concentration of CO_2 in the Arctic atmosphere reached 422.06 ppm, which was 2.08 ppm higher than the global average. Compared to 2022, the annual average concentration increased by 1.93 ppm.

During this period, the CH_4 concentration in the Arctic atmosphere also showed a stable year-on-year increase (Figure 3.4b), with an average growth rate of 7.5 ppb/year. In 2023, the annual average concentration of CH_4 in the Arctic atmosphere reached 2013.75 ppb, which was 79.75 ppb higher than the global average. Compared to 2022, it increased by 9.95 ppb.

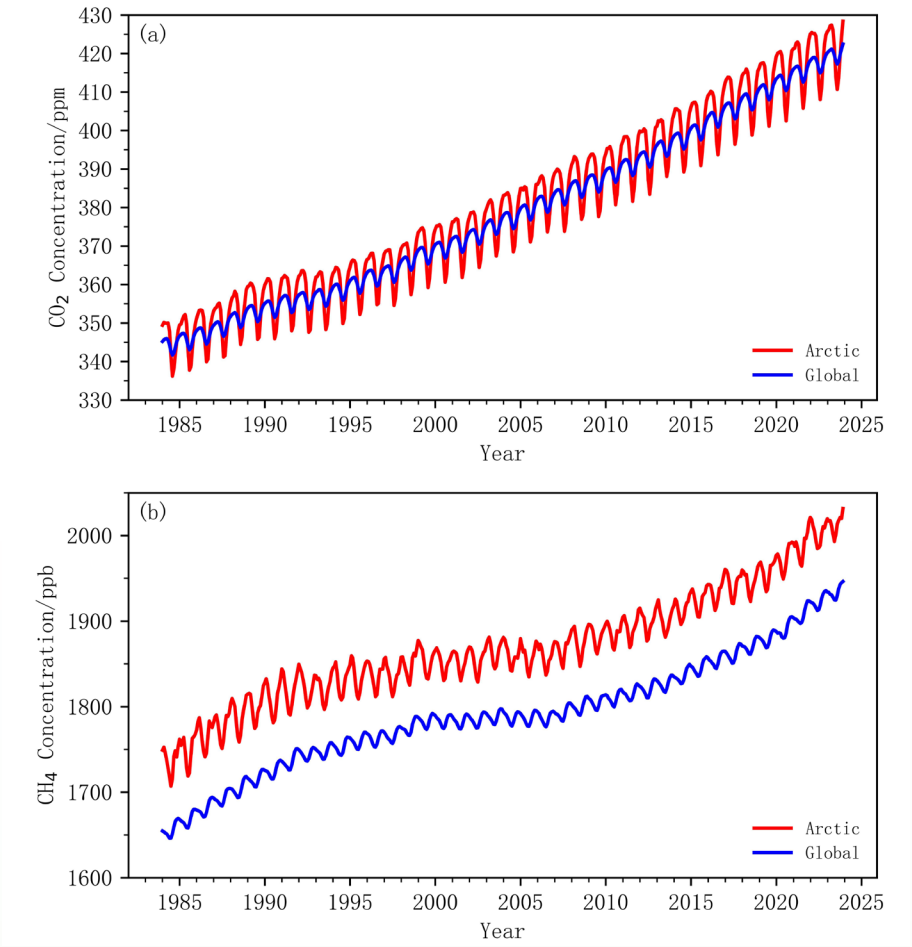

Figure 3.4 Changes in concentrations of CO_2 (a) and CH_4 (b) in in the Arctic and the globe, 1984 to 2023

(2) N_2O and SF_6

Currently, N_2O is monitored at six global atmospheric background stations in the Arctic. The annual average concentration of N_2O at these stations increased from 313.31 ppb in 1997 to 337.03 ppb in 2023, with an annual growth rates of 0.89 ppb/year (Figure 3.5a). In 2023, the annual average concentration of N_2O in the Arctic increased by 0.95 ppb compared to 2022.

The annual average concentration of SF_6 in six Arctic stations monitoring SF_6 increased from 4.22 ppt in 2002 to 11.69 ppt in 2023, with an average growth rate of 0.31 ppt/year(Figure 3.5b). In 2023, the annual average concentration of SF_6 in the Arctic increased by 0.41 ppt compared to 2021.

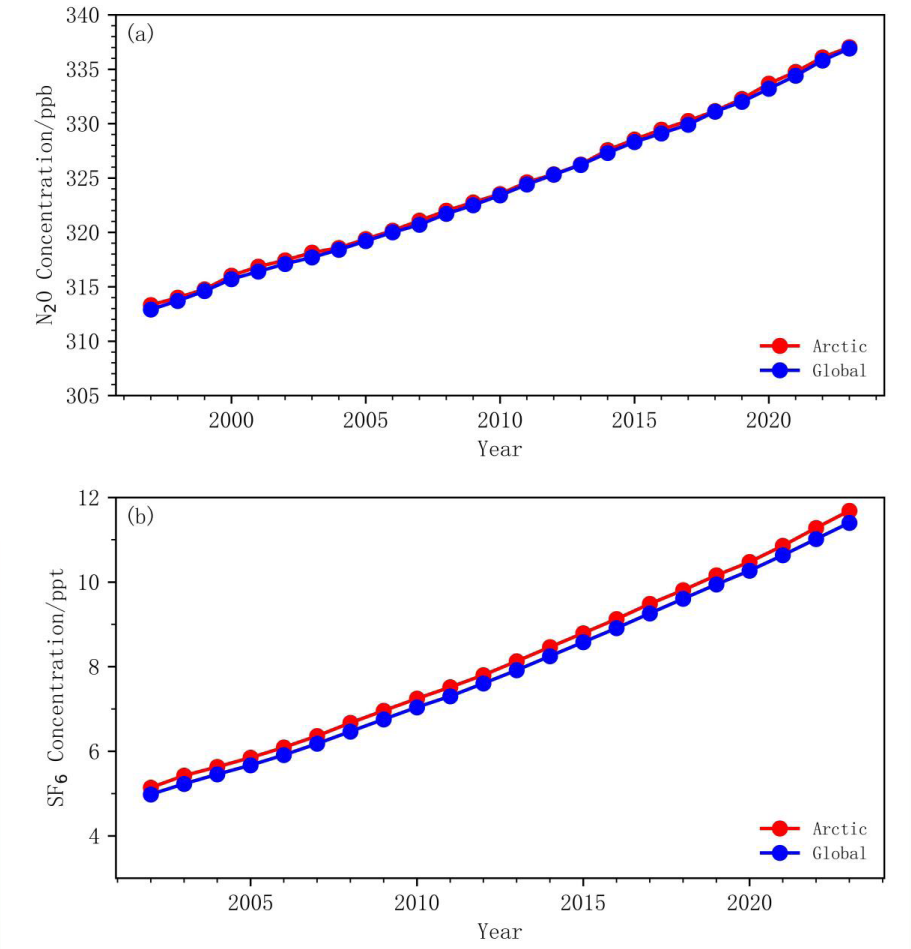

Figure 3.5 Annual average concentrations of (a) N_2O (1997–2023) and (b) SF_6 (2002– 2023) in the Arctic
Note: the global average concentration of SF_6 is from NOAA

3.2 Trace Gases

Trace gases refer to the atmospheric constituents that exist in extremely low concentrations, typically less than 1 ppm. Despite their minuscule proportion in the atmosphere, these gases play a crucial role in climate change, air pollution, and atmospheric chemical processes. Common trace gases include ozone (O_3), carbon monoxide (CO), and nitrogen oxides (NOx). This section analyzes surface ozone monitoring data from polar sites and China's Zhongshan Station, provided by the World Data Center for Reactive Gases (WDCRG). The data includes six stations in Antarctica and four in the Arctic, spanning the period from 1996 to 2023 (the surface ozone concentration data is available up to 2023). The main focus of this section is the temporal and spatial variations of surface ozone concentrations.

3.2.1 Antarctica

In 2023, surface ozone concentrations in Antarctica exhibited significant temporal and spatial variations. Inland stations, such as the South Pole and Concordia stations, recorded higher concentrations, with an

average concentration of 28.06 ppb. Coastal stations, including Zhongshan, Halley, Neumayer, and Syowa stations, displayed lower concentrations, with an average of 25.89 ppb. Notably, the ozone concentration at Zhongshan Station showed a significant decline starting in 2018, with an annual average decrease of 0.80 ppb/year, reaching an average concentration of 21.87 ppb in 2023. Overall, no significant long-term trend was observed in the surface ozone concentrations in Antarctica.

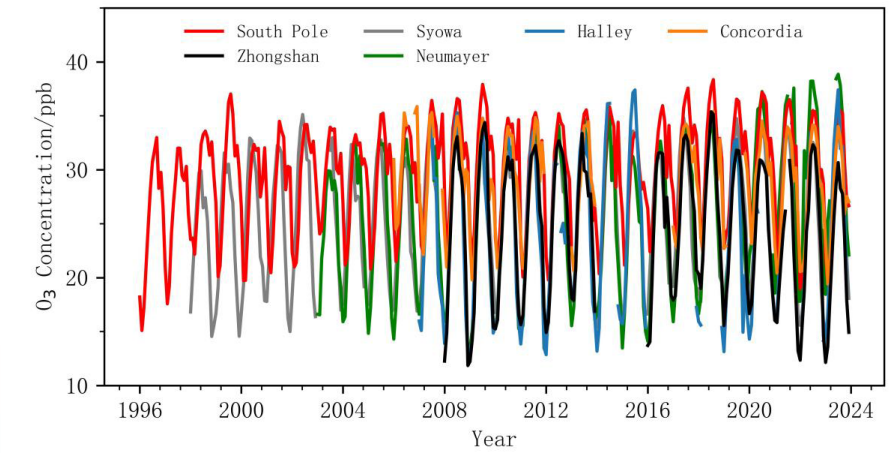

Figure 3.6 Time series of monthly average surface ozone concentrations from 1996 to 2023 at six atmospheric baseline stations in Antarctica

3.2.2 Arctic

In the Arctic, the average surface ozone concentration at the four stations increased from 32.92 ppb in 2000 to 35.34 ppb in 2023, with a change rate of approximately 0.11 ppb/year. In 2023, the surface ozone concentration in the Arctic increased by 1.60 ppb compared to 2022. However, since 2000, the average surface ozone concentrations in different regions of the Arctic have varied considerably. For example, the highest recorded average concentration at the Summit Station reached 45.22 ppb, while the average concentration at Barrow Station during the same period was only 27.42 ppb.

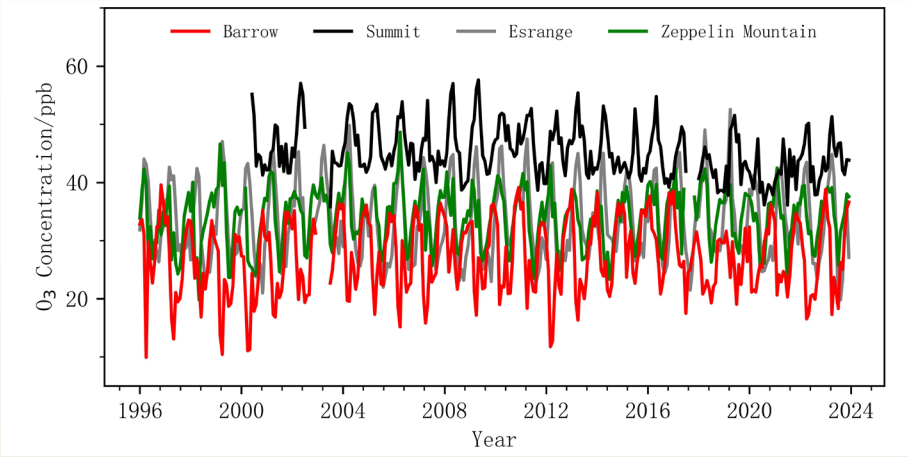

Figure 3.7 Time series of monthly average surface ozone concentrations from 1996 to 2023 at four atmospheric baseline stations in the Arctic

3.3 Total Ozone

3.2.1 Antarctic ozone hole

In 2024, the development of the Antarctic ozone hole was relatively stable, showing a moderation compared to the unusually large and persistent ozone hole phenomena observed in the previous four years. This year's ozone hole formed at the end of August, slightly later than the mid-August formation of the previous year. Notably, two rare stratospheric sudden warming events in July and August influenced the development of the ozone hole. With a rapid increase in ozone depletion, the ozone hole quickly expanded to 1.5×10^7 km² in early September, nearly covering the entire Antarctic continent. On September 28, the ozone hole reached its maximum daily coverage of approximately 2.2×10^7 km²; this value is lower than the approximately 2.5×10^7 km² observed in 2023 and 2022, more closely aligning with the average from 1979 to 2021.

Compared to previous years, the closing process of the ozone hole also showed more stability. Throughout October, the ozone hole continued to shrink steadily. With the stability of the polar vortex, the ozone hole remained at about 1.0×10^7 km² in November, significantly lower than the levels seen in 2023 and 2022. Furthermore, the ozone hole rapidly closed in early December, nearly coinciding with the average closing date from 1979 to 2021, and notably earlier than in previous years (since 2019, the ozone hole has typically closed in the latter half of December).

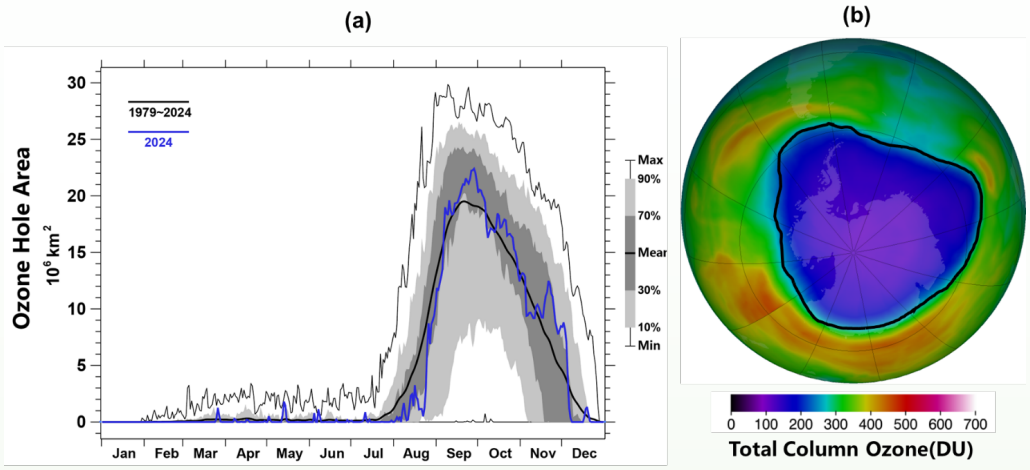

Figure 3.8 (a) Changes in the area of the Antarctic ozone hole in 2024 and comparison with the historical average (b) Maximum single-day area of the Antarctic ozone hole in 2024

3.2.2 Total column ozone in Arctic

In March 2024, the ozone column concentration in the Arctic region reached a record high of 477 Dobson Units (DU), marking the highest level recorded since 1979. This value is 14.5% higher than the average from 1979 to 2023. The primary cause of this extreme value was a series of large-scale planetary wave events during the winter of 2023-2024, which weakened the polar vortex and led to an abnormal increase in ozone levels. Throughout March, multiple daily records were set.

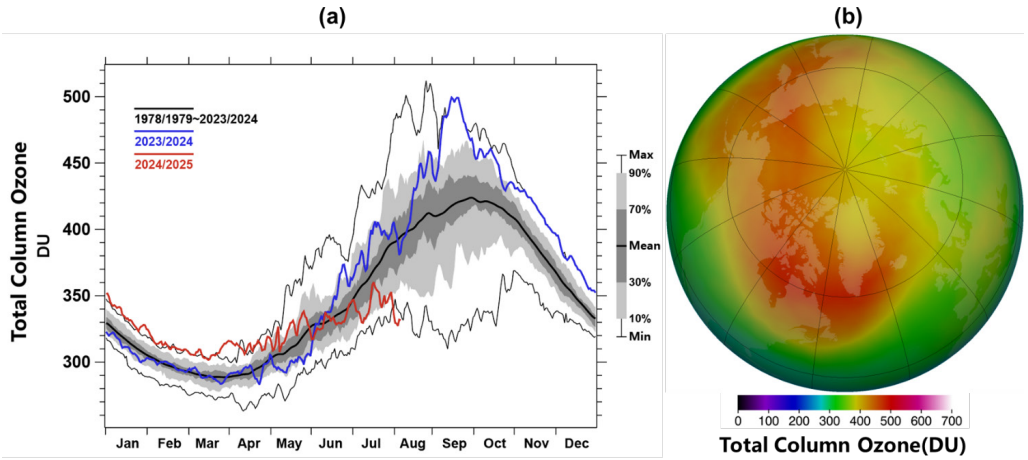

Figure 3.9 (a)Total ozone average for the Arctic region (north of 63°N) in 2024 compared to the historical average (b)Spatial distribution of Arctic mean total ozone in March 2024

Main Data Sources

1. National Arctic and Antarctic data center(NAADC) Meteorological observation products
   https://datacenter.chinare.org.cn/data-center/dindex
2. China Meteorological Administration Global Atmospheric/Land Surface Reanalysis data (CMA-RA)
   http://idata.cma/idata/web/fact/toTechReport2
3. Global Historical Climatology Network - Daily (GHCN-Daily)
   https://www.ncdc.noaa.gov/cdo-web/datasets
4. Global Surface Summary of the Day
   https://registry.opendata.aws/noaa-gsod
5. The British Antarctic Survey
   https://www.bas.ac.uk/project/reader/#data
6. Danish Meteorological Institute
   http://research.dmi.dk/data/
7. The Operational Sea Surface Temperature and Sea Ice Analysis (OSTIA) dataset
   https://data.marine.copernicus.eu/product/SST_GLO_SST_L4_REP_OBSERVATIONS_010_011/description
8. National Snow and Ice Data Center
   https://nsidc.org/data/nsidc-0051/versions/2
9. National Satellite Meteorological Center-FENGYUN Satellite Data
   http://data.nsmc.org.cn/portalsite/default.aspx
10. Daily Sea Ice Concentration of FY-3 MWRI of the -FENGYUN series satellites, provided by Sun Yat-sen University
    http://www.orsc.hellosea.org.cn/#/product-detail?ProductId=1896894818039107586
11. The Earth Science Data Systems of NASA (National Aeronautics and Space Administration)
    https://www.earthdata.nasa.gov/
12. Ocean University of China (OUC)
    http://coas.ouc.edu.cn/pogoc/sjgx/list.htm 11
13. The World Data Centre for Greenhouse Gases (WDCGG)
    https://gaw.kishou.go.jp/publications/global_mean_mole_fractions#content1
14. National Oceanic and Atmospheric Administration（NOAA）
    https://gml.noaa.gov/ccgg/data/getdata.php?gas=SF6
15. The World Data Center for Reactive Gases (WDCRG)
    https://ebas-data.nilu.no
16. Goddard Space Flight Center of NASA (National Aeronautics and Space Administration)
    https://ozonewatch.gsfc.nasa.gov/

Glossary

Antarctica: The vast region south of latitude 60°S.

Arctic: The vast region north of latitude 60°N.

Anomaly: The difference between a variable and its multi-year average value for the period 1991 to 2020.

Reanalysis Data: Historical weather data obtained by assimilating model forecasts and observational data through advanced, fixed assimilation systems and numerical forecast models to produce a rich dataset with complete spatial coverage and consistent time series. In this report, reanalysis data specifically refers to the first-generation global atmospheric reanalysis dataset, CMA-RA, released by the National Meteorological Information Center.

Southern Ocean: Refers to a unique body of water that surrounds the Antarctic continent and has no land boundary to the north. It is composed of parts of the South Pacific, South Atlantic and South Indian Oceans, together with the Weddell Sea, Ross Sea, Amundsen Sea and Bellingshausen Sea around the Antarctic continent, covering the area south of 50°S.

The Arctic Ocean: Its main body is located north of the Arctic Circle (66.5°N), and the latitude of its core sea area ranges from 65°N to 90°N.

Antarctic Oscillation(AAO): The seesaw change phenomenon of the pressure field between the Antarctic and the mid-latitudes of the Southern Hemisphere, also known as the Southern Hemisphere Annular Model (SAM), is one of the main characteristic modes of atmospheric circulation in the Southern Hemisphere.

Arctic Oscillation(AO): The seesaw change phenomenon of the air pressure field between the Arctic and the mid-latitudes of the Northern Hemisphere, also known as the Northern Hemisphere Annular Mode(NAM), is one of the main characteristic modes of atmospheric circulation in the Northern Hemisphere.

AAO/AO index: Using CMA-RA reanalysis data, it is calculated based on the difference in zonal mean sea level pressure between the polar area and the middle latitudes (Li et al,2003). The AO index is the difference between 35°N and 65°N, and the AAO index is the difference between 40°S and 70°S.

Polar Vortex: a large-scale low-pressure vortex phenomenon in the polar troposphere and stratosphere, which has an important impact on the climate of the polar regions and mid-high latitudes of the northern and southern hemispheres.

Arctic Polar Vortex Index: Indicators used to describe and measure the characteristics and changes of the Arctic polar vortex.

Sea ice concentration: a measurement of the amount of sea ice in a given area, usually described as a percentage.

Sea ice extent: the total region with at least 15 percent sea ice concentration.

Melt Onset(MO): Free water is continuously present with in the snow pack and the ice surface becomes

damp at the snow ice interface.

Freeze Onset(FO): The ice is generally bare to lightly snow covered, well drained and the surface layer of the ice is refrozen.

Greenhouse gases: Natural or anthropogenic gas components in the atmosphere that can absorb and emit longwave radiation from the Earth's surface, atmosphere, and clouds, leading to the greenhouse effect. The major greenhouse gases in the Earth's atmosphere include carbon dioxide (CO_2), methane (CH_4), nitrous oxide (N_2O), sulfur hexafluoride (SF_6), hydrofluorocarbons (HFCs), and perfluorocarbons (PFCs), as specified in the Kyoto Protocol.

PPM: The number of molecules of a given gas per million (10^6) molecules of dry air

P**PB:** The number of molecules of a given gas per billion (10^9) molecules of dry air.

PPT: The number of molecules of a given gas per trillion (10^{12}) molecules of dry air.

Greenhouse Gases observation stations in Arctic: Kotelny Island Station (Russia, KOT), Tiksi Station (Russia, TIK), Alert Station (Canada, ALT), Mould Bay Station (Canada, MBC), Barrow Station (USA, BRW), Behchokǫ̀ Station (Canada, BCK), Cambridge Bay Station (Canada, CBY), Inuvik Station (Canada, INU), Zeppelin Mountain Station (Norway, ZEP), Summit Station (Denmark, SUM), Teriberka Station (Russia, TER), Pallas Station (Finland, PAL), Storhofdi Station (Iceland, ICE), Lerwick Station (UK, SIS), Ocean Station Charlie (USA, STC)

Greenhouse Gases observation stations in Antarctica: King Sejong Station (South Korea, KSG), Jubany Station (Argentina, JBN), Palmer Station (USA, PSA), Casey Station (Australia, CYA), Mawson Station (Australia, MAA), Showa Station (Japan, SYO), Halley Station (UK, HBA), Arrival Heights Station (New Zealand, ARH), McMurdo Station (USA, MCM), South Pole Station (USA, SPO), Zhongshan Station (China, ZOS).

Dobson unit (DU): A unit to measure the total amount of ozone in a vertical column above the Earth's surface (total column ozone). The number of Dobson Units is the thickness in units of 10-5 m that the ozone column would occupy if compressed into a layer of uniform density at a pressure of 1013 hPa and a temperature of 0°C. One DU corresponds to a column of ozone containing 2.69×10^{20} molecules per square metre. A typical value for the amount of ozone in a column of the Earth's atmosphere, although very variable, is 300 DU.

Ozone-depleting substances (ODSs): Ozone-depleting substances (ODSs) are man-made gases that destroy ozone (O_3) once they reach the ozone layer in the stratosphere. Ozone depleting substances include: chlorofluorocarbons (CFCs), hydrochlorofluorocarbons (HCFCs), hydrobromofluorocarbons (HBFCs), halons, methyl bromide, carbon tetrachloride and methyl chloroform.

Ozone layer: The ozone layer is a layer of Earth's stratosphere that absorbs most of the Sun's ultraviolet radiation. It contains high concentrations of ozone (O_3) in relation to other parts of the atmosphere, although still small in relation to other gases in the stratosphere.The ozone layer is mainly found in the lower portion of the stratosphere, from approximately 12 to 40 kilometres above Earth, and reach the maxima from 20 to 25 kilometres. Every year, during the spring of the Southern Hemisphere, the ozone layer over the Antarctic region experiences very strong depletion, caused by anthropogenic chlorides and bromides in combination with the region's specific meteorological conditions. This phenomenon is known as the ozone hole.

STATE OF POLAR CLIMATE
2024